

Contextual Stochastic Optimization for Omnichannel Multi-Courier Order Fulfillment Under Delivery Time Uncertainty

Tinghan Ye, Sikai Cheng, Amira Hijazi, Pascal Van Hentenryck
NSF AI Institute for Advances in Optimization (AI4OPT), Georgia Institute of Technology, Atlanta, GA

Abstract. *Problem definition:* The paper studies a large-scale order fulfillment problem for a leading e-commerce company in the United States. The challenge involves selecting fulfillment centers and shipping carriers with observational data only to efficiently process orders from a vast network of physical stores and warehouses. The company’s current practice relies on heuristic rules that choose the cheapest fulfillment and shipping options for each unit, without considering opportunities for batching items or the reliability of carriers in meeting expected delivery dates. *Methodology / results:* The paper develops a data-driven Contextual Stochastic Optimization (CSO) framework that integrates distributional forecasts of delivery time deviations with stochastic and robust order fulfillment optimization models. The framework optimizes the selection of fulfillment centers and carriers, accounting for item consolidation and delivery time uncertainty. Validated on a real-world data set containing tens of thousands of products, each with hundreds to thousands of fulfillment options, the proposed CSO framework significantly enhances the accuracy of meeting customer-expected delivery dates compared to current practices. It provides a flexible balance between reducing fulfillment costs and managing delivery time deviation risks, emphasizing the importance of contextual information and distributional forecasts in order fulfillment. *Managerial implications:* This is the first paper that studies the omnichannel multi-courier order fulfillment problem with delivery time uncertainty through the lens of contextual optimization, fusing machine learning and optimization. The results provide actionable insights for e-commerce companies and online retailers to enhance service quality and customer satisfaction through efficient order fulfillment strategies that accounts for delivery time uncertainty. Adopting this framework can balance cost effectiveness with customer service, potentially leading to higher customer retention and profitability.

Funding: This research was partly supported by the NSF AI Institute for Advances in Optimization (Award 2112533).

Key words: logistics, order fulfillment, machine learning, contextual stochastic optimization, contextual robust optimization

1. Introduction

Over the past decade, online shopping has surged dramatically. The e-commerce share of total retail sales in the United States has risen from 6% in 2015 to 16% in 2024, exceeding 1.1 trillion dollars (US Department of Commerce 2024). Amid intense competition in pricing, service, and marketing, driven by the lucrative e-commerce market, logistical performance has become a key element to success. Last-mile fulfillment, in particular, is critical as it accounts for 55% of the total transportation costs in the fulfillment process (Viswanathan 2023). This evolving market landscape poses unprecedented challenges for e-commerce companies striving to deliver satisfactory customer services. Fortunately, the growing volume of data also offers opportunities for data-driven operational improvements, enabling companies to boost revenue and cut costs (Fisher et al. 2019).

In addition, after the COVID-19 pandemic, the demand for timely home delivery has also increased significantly. As a result, omnichannel fulfillment and the use of multiple couriers, including crowd-shipping, have become essential components of the fulfillment landscape, drawing significant attention both in industry and academia (Dethlefs et al. 2022, Mohri et al. 2023, Das et al. 2023). The omnichannel approach combines distribution centers (DCs) and brick-and-mortar stores to fulfill online orders. Unlike the traditional method that uses DCs for online orders and stores for in-store purchases separately, the omnichannel approach leverages the proximity of physical stores to delivery addresses. This can potentially offer more cost-effective and faster delivery options for online customers (Acimovic and Farias 2019). Meanwhile, in the crowd-shipping model, retailers recruit non-dedicated drivers, such as gig couriers like Roadie, to handle pick-up and delivery tasks for online customers. This approach can alleviate the workload of employed drivers during peak hours and offer faster delivery to customers, resulting in higher service satisfaction (Zehtabian et al. 2022, Behrendt et al. 2023). *The problem considered in this paper involves fulfilling orders by choosing from various types of fulfillment centers, such as warehouses and stores, and different couriers, including traditional shipping companies and gig couriers.*

Given that transportation and shipping are significant cost drivers in e-commerce (Dethlefs et al. 2022, Kuhn and Sternbeck 2013, Hübner et al. 2013), delivery consolidation has emerged as an effective strategy for fulfilling orders with multiple items. This approach has been shown to enhance consumer satisfaction (Wagner et al. 2023), while also reducing shipping costs for online retailers (Chen et al. 2024). In addition to cutting parcel expenses, item consolidation enhances the customer experience by eliminating the need to receive multiple packages for a single order. This approach not only improves convenience but also promotes a more sustainable and environmentally friendly fulfillment process by decreasing the number of packages shipped and the number of delivery trips needed. This reduction in shipments and trips leads to lower carbon emissions and less packaging waste, contributing to greener logistics practices (Ülkü 2012). *This paper also investigates multi-item order consolidation in its omnichannel fulfillment problem.*

Most existing studies on order fulfillment optimization have not explicitly considered the uncertainty in delivery timeliness. However, Freedman (2019) highlight the strong desire of customers for accurate delivery time promises and faster service. The survey indicates that around 44% of online shoppers have abandoned their shopping carts because the items they wanted would not arrive on time, while 20% abandon orders with unclear delivery dates. Furthermore, 28% of shoppers are willing to pay for expensive, expedited shipping to receive products at their desired time. The statistics clearly show that customers prioritize service quality, sometimes even more than the product value, when making purchase decisions. Moreover, Salari et al. (2022) point out the importance of considering delivery time uncertainty in order fulfillment to better meet customer expectations and improve satisfaction. Their proposed promised delivery time policy demonstrates a 6.1% increase in sales volume in numerical experiments. Notably, overpromising delivery

times can lead to higher return rates, lower repurchase rates, and dissatisfaction with delayed service. Additionally, customers can have mixed sentiments over underpromised delivery times, as early deliveries may not align with their availability. Therefore, missing the exact promised delivery date can negatively impact short-term and long-term sales, both implicitly and explicitly (Salari et al. 2022, Cui et al. 2024). *Given the crucial role of delivery timeliness, the paper incorporates delivery time uncertainty into the omnichannel multi-courier order fulfillment optimization problem through a contextual stochastic optimization framework.*

One of the key challenges of Omnichannel Multi-Courier Order Fulfillment Optimization comes from the nature of historical data: only observational data—i.e., delivery time deviations for the fulfillment options actually chosen—are available. Counterfactual deviations for unchosen options are never observed, similar to the bandit feedback setting (Lattimore and Szepesvári 2020). *The availability of observational data only, raises fundamental challenges that are typically not addressed in prior work.*

To address these challenges, *this paper proposes a Contextual Stochastic Optimization (CSO) framework, encompassing both risk-neutral and robust approaches.* Unlike traditional stochastic programming methods that depend on static, predefined probability distributions for uncertainties, CSO combines machine learning techniques with mathematical optimization to dynamically predict uncertainties based on contextual information. Thanks to the availability of contextual information, CSO has the flexibility of generating more tailored and effective decisions, leveraging the most current and relevant information. Such flexibility is particularly beneficial in the dynamic environment of online retail, where conditions and customer behaviors can change rapidly, requiring a more responsive approach to decision making. The effectiveness of CSO has been validated in the existing operations research and management science literature (Mišić and Perakis 2020, Sadana et al. 2024). This approach has proven successful in various applications, including inventory control (Bertsimas et al. 2016, Meller et al. 2018), price and revenue management (Ito and Fujimaki 2016, Perakis et al. 2023), and, more recently, school redistricting (Guan et al. 2024).

1.1. Contributions

The key novelty in this paper is a CSO framework for an omnichannel multi-courier order fulfillment optimization with observational data only. Existing studies on CSO typically assume the availability of a dataset $\mathcal{D} = \{(\mathbf{s}_1, \mathbf{c}_1), (\mathbf{s}_2, \mathbf{c}_2), \dots\}$, pairing covariates with fully observed uncertain parameter vectors. However, real-world scenarios often involve high-dimensional uncertain parameters where individual data points capture only partial information, particularly when uncertainty measurement depends on the chosen solution, which is the case in the application considered in this paper.

To address the challenge of observational data, this paper introduces a generalized CSO framework addressing these real-world complexities. *The novel CSO framework is applied to a sophisticated stochastic*

omnichannel order fulfillment optimization problem with multiple carrier options and delivery time uncertainties. In collaborating with a major US online retailer, the framework is rigorously evaluated on an industrial order fulfillment dataset featuring a vast, intricate fulfillment network. This application demonstrates the framework capabilities and its potential impact on large-scale, real-world optimization challenges. The contributions of the paper can be summarized as follows.

1. *Generic CSO framework for observational data:* The paper presents a novel, distribution-agnostic contextual stochastic optimization (CSO) framework that converts problems with missing-counterfactual observational data into tractable problems. A contextual distribution oracle is learned from partial observations, and the resulting problem is solved via two scalable solution paradigms—Contextual Sample Average Approximation (C-SAA) and Contextual Robust Optimization (C-RO).

2. *Tailored contextual distribution learning for e-commerce delivery time deviations:* The paper adapts calibrated probabilistic multi-class classification and tree-based quantile regression to exploit the discrete, ordinal nature of delivery time deviations, yielding well-calibrated contextual distributions for the CSO framework.

3. *Consolidation- and timeliness-aware MILP for omnichannel, multi-courier fulfillment:* The paper proposes the first data-driven mixed-integer linear program (MILP) that jointly selects fulfillment centers and carriers and captures item-consolidation discounts while embedding learned contextual deviation distributions in a tractable way.

4. *Industry-scale real-world validation:* The paper includes an extensive case study at a major e-commerce retailer to (1) validate the efficacy of the proposed approaches in reducing expected fulfillment costs and (2) show significant improvements in on-time delivery rates compared to standard heuristics and baseline models. These results demonstrate the potential for substantial real-world impact.

1.2. Structure of the Paper

The remainder of this paper is organized as follows. Section 2 reviews related literature. Section 3 formulates the omnichannel multi-courier order-fulfillment problem under delivery-time deviation uncertainty. Section 4 develops a generic contextual stochastic optimization framework for observational data and introduces two tractable solution paradigms—Contextual Sample Average Approximation and Contextual Robust Optimization. Section 5 describes the machine-learning methods (multi-class classification and tree-based quantile regression) used to implement the contextual distribution oracle. Section 6 presents the case study, computational results, and actionable insights from a real dataset. Finally, Section 7 concludes and outlines directions for future research.

2. Related Literature

There are several streams of literature related to this paper in terms of methodology and problem context.

2.1. Data-Driven Decision Making

This paper adds to the growing body of literature on data-driven decision-making, particularly at the intersection of machine learning and optimization, which has led to the development of CSO. Sadana et al. (2024) put forth a comprehensive survey on contextual optimization. Tutorials on various methodologies and applications of CSO models in logistics and operations management are available in the works of Mišić and Perakis (2020), Qi and Shen (2022), and Tian et al. (2023). Among the body of research on CSO, the most relevant to this paper are those that focus on learning contextual distributions of uncertain parameters and incorporating these forecasts into optimization models. Data-driven approaches typically build these forecasts from empirical residual errors (Deng and Sen 2022, Kannan et al. 2023, Perakis et al. 2023) or weighted empirical distributions based on proximity to the training data (Bertsimas and Kallus 2020, Notz and Pibernik 2022). However, these studies assume full observation of uncertain parameters for each data point, which differs from the context of this paper. Recent research has also explored integrating downstream optimization effects into ML model training. Elmachtoub and Grigas (2022) introduce the Smart Predict then Optimize (SPO) loss and its convex surrogate for point prediction models, with subsequent extensions to contextual distributional estimation (Qi et al. 2021, Kallus and Mao 2023). However, the SPO loss framework is not directly applicable to this paper’s context, as the dataset analyzed here is observational. In such datasets, outcomes are only partially observed based on decisions made, presenting unique challenges not addressed by these existing methods.

This paper thus contributes to the field of data-driven decision-making that handles observational data, a domain explored by prior research, e.g., in Bertsimas et al. (2019) and Jo et al. (2021), using optimal prescriptive trees for prescriptive analytics in personalized treatment. While these methods effectively learn policies mapping features to actions, they cannot be directly applied to the fulfillment problem considered in this paper due to the presence of instance-specific hard constraints on decisions. The proposed framework addresses these limitations, offering a novel approach to CSO problems with observational data and constrained decision spaces.

Unlike earlier CSO applications that focus on risk-neutral objectives, a growing stream of research is concerned with risk-averse optimization models that incorporate contextual information (Bayram et al. 2022, Peršak and Anjos 2023, Patel et al. 2024, Sun et al. 2024). Building on these studies, this paper also adapts traditional robust optimization models to tackle a unique CSO problem that differs from those explored in other research.

2.2. Order Fulfillment Problem

The novelty in this paper is the application of CSO to a unique instance of the order fulfillment problem. The order fulfillment problem has been extensively studied, and Acimovic and Farias (2019) provide a tutorial on related algorithms developed for addressing the fulfillment optimization problem. In terms of problem

context, the most relevant works are those related to omnichannel and multi-item order fulfillment (Xu et al. 2009, Acimovic and Graves 2015, Jasin and Sinha 2015, Zhao et al. 2020, Wei et al. 2021, Ma 2023, Chen et al. 2024). However, these works do not address fulfillment involving a variety of carrier shipping options.

Among the research on order fulfillment, demand uncertainty is the most commonly studied source of randomness (Jasin and Sinha 2015, Zhao et al. 2020, Das et al. 2023, DeValve et al. 2023, Ma 2023). In this paper, demand uncertainty is not considered because the focus is on a single-period order fulfillment problem, rather than a forward-looking approach that spans multiple periods.

A few studies do address delivery time uncertainty at various stages of the order fulfillment process or throughout the entire process. For instance, Raj et al. (2024) propose an integrated queuing model that accounts for delivery time uncertainty in different parts of the order life cycle. They incorporate these uncertainties into an optimization model that minimizes costs while adhering to a delivery probability constraint to ensure on-time delivery.

In contrast to using queuing models, this study is particularly relevant to data-driven, ML-based methods that address for delivery time uncertainty in order fulfillment. Specifically, Liu et al. (2021) integrate point predictions of travel time with a last-mile delivery order assignment optimization problem. They propose both a SAA model and a distributionally robust optimization (DRO) model, with the latter constructing a moment-based ambiguity set. Similarly, Kandula et al. (2021) explore a last-mile delivery problem, focusing on delivery success as the uncertainty. They map success probabilities to delivery times, which are then integrated into a Vehicle Routing Problem with Time Windows. Bayram et al. (2022) study a robust order batching optimization problem in warehouse picking and packing. They use random forest to predict order processing time to form an uncertainty set within a robust optimization model. This paper builds on similar concepts, developing tractable approximations and reformulations of integer programming-based optimization models. More precisely, the uncertainty in the order fulfillment problem considered in this paper is the potential order delivery deviations, which can occur at various stages of the fulfillment process. A similar uncertainty addressed using data-driven approach can be found in Salari et al. (2022), who develop a quantile regression forest-based method to generate distributional forecasts of order delivery times. Their approach then applies a decision rule, designed to balance the asymmetric costs of early and late deliveries, to produce expected arrival times for customers. This paper differs in two key aspects. First, the distributional forecasts are directly incorporated into contextual optimization models, eliminating the need for a separate decision rule to generate point predictions. Second, the CSO framework proposed in this paper is more comprehensive, accommodating multiple carrier options, whereas Salari et al. (2022) focus on a single-carrier scenario.

3. The Omnichannel Multi-Courier Order Fulfillment Problem

This section introduces a real-world order fulfillment problem encountered by the industrial partner.

3.1. High-Level Problem Description

This section provides a high-level overview of the online order fulfillment challenges faced by the industrial partner. Similar to other major e-commerce companies, tens of thousands of orders are placed continuously throughout the day on the website and await processing. Each incoming order is organized by stock-keeping units (SKUs), resulting in one or more order lines. For each order line, there are hundreds of fulfillment centers across the company network eligible to source the SKUs. These centers include primarily physical stores, as well as regional distribution centers and metro e-commerce centers. Each location is equipped with multiple eligible carriers capable of providing different levels of service, such as Ground, Same-Day, and Overnight shipping. Throughout this paper, “carrier” refers to one of these specific carrier-service pairs. The set of available carriers spans from major shipping companies to crowdsourced gig carriers. Figure 1 illustrates the order fulfillment life cycle within the operations of the industrial partner.

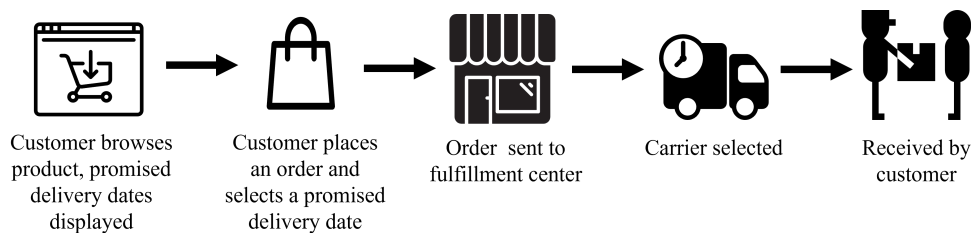


Figure 1 The Life Cycle of the Order Fulfillment Process.

Before making an order fulfillment decision, the company has access to both the transactional details of the order and the real-time status of the fulfillment network. Specifically, the order information includes the date and time the order was placed, the type, dimensions, weight, and quantities of the SKUs, the shipping destination, and the desired delivery date. The network status data provides details on the on-hand inventory levels of the requested SKUs and the remaining open capacities at various fulfillment centers. In addition, each carrier provides an estimated table for shipping costs and planned time-in-transit.

Given this information, the problem is to decide which fulfillment center to source each order line from and which carrier to use for shipping from that location. The goal is to identify the most cost-effective fulfillment option (a location-carrier pair) while ensuring the customer’s desired delivery date is met. The uncertainty of this problem lies in the delivery timeliness performance of each fulfillment option.

3.1.1. Overview of the Current Practice Currently, the industrial partner uses a sourcing engine that employs a straightforward greedy algorithm. For each unit in an order, the sourcing engine sorts the eligible location-carrier pairs by the estimated shipping costs and transit times.

There are several limitations with this approach. First, since the engine makes decisions for each unit independently, it misses the opportunity to consolidate multiple units of the same or different products within an order. This can lead to higher shipping costs, as the potential to reduce the number of packages—and thereby lower shipping expenses—is not fully realized.

Second, the method relies solely on static transit time estimates provided by the carriers based on their service levels to select the best carrier for meeting the promised delivery date. This approach assumes that these estimates are always accurate. However, static transit times may not accurately reflect the actual delivery performance of carriers. Historical data from the industrial partner reveals that over 10% of orders experience varying degrees of early or late deliveries, which are called *deviations* in this paper. Given the complexity of the entire fulfillment process, these deviations can be attributed to numerous factors, such as warehouse pick-and-pack performance, late carrier arrivals, no-shows, and external factors like extreme weather or other unexpected circumstances. Such deviations from customer expectations can negatively impact their experience, potentially harming the company in the long run.

3.2. The Nominal Optimization Problem

This section introduces the nominal MILP model developed for optimizing the omnichannel multi-courier order fulfillment problem. A comprehensive list of the notations presented in this section is provided in Appendix for reference.

3.2.1. Main Decision Variables Let \mathcal{I} be the set of SKUs and \mathcal{V} be the set of fulfillment options. Here, \mathcal{V} is defined as the Cartesian product $\mathcal{K} \times \mathcal{L}$, where \mathcal{K} denotes the set of carriers, and \mathcal{L} denotes the set of locations.

Each order needs to solve an independent optimization problem to decide the selection of carrier-location pairs for each SKU. The primary decision variables are denoted by the vector $\mathbf{z} = (z_{ik\ell})_{i \in \mathcal{I}, k \in \mathcal{K}, \ell \in \mathcal{L}}$, where each $z_{ik\ell} \in \mathbb{Z}$ indicates the quantity of SKU i sourced from location ℓ and shipped by carrier k .

3.2.2. Objective Function The objective of the optimization problem for an order is to minimize the overall fulfillment costs while ensuring timely delivery. The fulfillment costs for an order include the fixed sourcing (non-parcel) costs and the shipping (parcel) costs, with consolidation discounts applied when multiple units are assigned to the same carrier-location pair. Delivery timeliness is measured by deviations from the desired delivery date, whether early or late. To encourage timeliness, the objective imposes penalties for both early and late deliveries.

The objective function is formally defined as follows. Let $c_{ik\ell}^{ship} > 0$ be the per-unit shipping cost when using location ℓ and carrier k to fulfill SKU i . For each location ℓ , let $c_{\ell}^{fixed} > 0$ be the per-unit fixed sourcing cost. For each carrier k , let $\beta_k \in (0, 1)$ be the discount percentage applied to shipping costs when multiple units are shipped using carrier k from the same fulfillment center. Let $\gamma^+ \geq 0$ and $\gamma^- \geq 0$ be constants that convert late and early delivery penalties into per-unit costs, respectively.

In an ideal setting where all carrier-location deviations are known at the time of fulfillment, let the vector $\mathbf{d} = (d_{k\ell})_{k \in \mathcal{K}, \ell \in \mathcal{L}}$ represent the realized uncertain delivery deviations, where each $d_{k\ell}$ denotes the number of days that the carrier-location pair (k, ℓ) deviates from desired delivery date. A positive deviation indicates late delivery, a zero deviation indicates on-time delivery, and a negative deviation indicates early delivery.

The weighted objective function for an order can be constructed as follows:

$$g(\mathbf{z}, \mathbf{d}) = \begin{cases} \sum_{i \in \mathcal{I}} \sum_{k \in \mathcal{K}} \sum_{\ell \in \mathcal{L}} [c_{\ell}^{fixed} + (1 - \beta_k) c_{ik\ell}^{ship} + \gamma^+ d_{k\ell}^+ + \gamma^- d_{k\ell}^-] z_{ik\ell} & \text{if } \sum_{i \in \mathcal{I}} z_{ik\ell} \geq 2, \\ \sum_{i \in \mathcal{I}} \sum_{k \in \mathcal{K}} \sum_{\ell \in \mathcal{L}} (c_{\ell}^{fixed} + c_{ik\ell}^{ship} + \gamma^+ d_{k\ell}^+ + \gamma^- d_{k\ell}^-) z_{ik\ell} & \text{otherwise,} \end{cases} \quad (1)$$

where $d_{k\ell}^+ = \max\{0, d_{k\ell}\}$ and $d_{k\ell}^- = \max\{0, -d_{k\ell}\}$. This objective function encourages item consolidation within an order by applying a carrier-specific discount if at least two units are sourced from the same location and shipped by the same carrier. In addition, it leverages an asymmetric penalty cost function for delivery deviations, where $\gamma^+ \gg \gamma^-$. This asymmetry strongly penalizes late deliveries to discourage delays while also applying a smaller penalty to disincentivize early deliveries. Specifically, the penalties can be interpreted as the opportunity cost associated with early deliveries and the lost-sale cost associated with late deliveries. The objective function is piecewise linear and can be linearized using standard rewritings.

3.2.3. Operational Constraints Several operational constraints ensure that the selection of fulfillment center locations and carriers is feasible in practice. For location $\ell \in \mathcal{L}$, let $\text{inv}_{i\ell} \geq 0$ be the inventory level of SKU i at location ℓ and $\text{cap}_{\ell} \geq 0$ be the available capacity at location ℓ when the order is placed. Let $q_i \geq 0$ be the quantity of SKU i in the order, and let $e_{ik\ell} \in \{0, 1\}$ be a binary indicator of whether the location-carrier pair (ℓ, k) is an eligible fulfillment option for SKU i . An assignment \mathbf{z} in the feasible set \mathcal{Z} must obey the following constraints.

- Each unit of an SKU must be sourced from exactly one location and shipped by exactly one carrier.

$$\sum_{k \in \mathcal{K}} \sum_{\ell \in \mathcal{L}} z_{ik\ell} = q_i, \quad \forall i \in \mathcal{I} \quad (2)$$

- Each SKU can only be fulfilled by eligible candidate location-carrier pairs, which may vary depending on the carrier's coverage and package requirements.

$$z_{ik\ell} \leq q_i e_{ik\ell}, \quad \forall i \in \mathcal{I}, k \in \mathcal{K}, \ell \in \mathcal{L} \quad (3)$$

- Only locations with available inventory of the requested SKUs can be chosen.

$$\sum_{k \in \mathcal{K}} z_{ik\ell} \leq \text{inv}_{i\ell}, \quad \forall i \in \mathcal{I}, \ell \in \mathcal{L} \quad (4)$$

- Each location has a daily capacity limit on the total number of units it can process.

$$\sum_{i \in \mathcal{I}} \sum_{k \in \mathcal{K}} z_{ik\ell} \leq \text{cap}_{\ell}, \quad \forall \ell \in \mathcal{L} \quad (5)$$

3.3. The Contextual Stochastic Order Fulfillment Problem

In practice, the delivery deviations of each carrier-location pair cannot be perfectly estimated in advance. To account for this uncertainty for each order, this section models the vector of uncertain delivery deviations $\tilde{\mathbf{d}} = (\tilde{d}_{k\ell})_{k \in \mathcal{K}, \ell \in \mathcal{L}} \sim \mathbb{P}$ as a $(|\mathcal{K}||\mathcal{L}|)$ -dimensional random vector governed by a joint probability distribution \mathbb{P} . Since deviations measured in days only take on discrete values in the dataset, each $\tilde{d}_{k\ell}$ inherently follows a discrete probability distribution. It is further assumed that every $\tilde{d}_{k\ell}$ shares the same finite, ordered support. To formalize this, let C be the total number of distinct deviation values and denote them by $\xi_1 < \xi_2 < \dots < \xi_C$. By definition, any realization $d_{k\ell}$ of $\tilde{d}_{k\ell}$ must lie in this set: $d_{k\ell} \in \{\xi_1, \xi_2, \dots, \xi_C\}$.

In addition, let $\mathbf{s} = (\mathbf{s}_{k\ell})_{k \in \mathcal{K}, \ell \in \mathcal{L}}$ denote the state vector observable to the order before the fulfillment decision is made, where each $\mathbf{s}_{k\ell}$ is a vector of covariates encompassing information about order details and fulfillment network status related to carrier-location pair (k, ℓ) . The contextual distribution of the deviation vector, upon observing \mathbf{s} , is denoted by $\mathbb{P}(\mathbf{d} \mid \mathbf{s})$, and the individual deviation contextual distribution is $\mathbb{P}_{k\ell}(d_{k\ell} \mid \mathbf{s}_{k\ell})$ for each $k \in \mathcal{K}$ and $\ell \in \mathcal{L}$.

This leads to the following contextual stochastic order fulfillment problem (CSOFP):

$$\text{(CSOFP)} \quad \min_{\mathbf{z} \in \mathcal{Z}} \mathbb{E}_{\tilde{\mathbf{d}} \sim \mathbb{P}(\mathbf{d} \mid \mathbf{s})} [g(\mathbf{z}, \tilde{\mathbf{d}})]. \quad (6)$$

Solving Problem (6) in practice requires leveraging data from past orders. Unlike classical CSO formulations where the entire random cost vector is observed, CSOFP is based on an observational dataset of past decisions and their realized costs. Let \mathcal{O} be the set of historical orders. For each $o \in \mathcal{O}$, define the decision vector $\mathbf{z}_o = (z_{ik\ell, o})_{i \in \mathcal{I}, k \in \mathcal{K}, \ell \in \mathcal{L}}$. Since deviations were observed only for chosen (i, k, ℓ) triples, the full deviation vector $\mathbf{d}_o = (d_{k\ell, o})_{k \in \mathcal{K}, \ell \in \mathcal{L}}$ contains many unobserved entries. The subset of realized deviations for order o is:

$$\mathbf{D}_o := \{d_{k\ell, o} \mid \sum_{i \in \mathcal{I}} z_{ik\ell, o} > 0, k \in \mathcal{K}, \ell \in \mathcal{L}\}.$$

The resulting dataset available for estimating the contextual distribution $\mathbb{P}(\mathbf{d} \mid \mathbf{s})$ is $\mathbb{D} = \{(\mathbf{s}_o, \mathbf{D}_o)\}_{o=1}^{|\mathcal{O}|}$.

4. Methodology: A Generic CSO Framework for Observational Data

Solving CSOFP under observational data requires: (1) learning a contextual distributional oracle from partial realizations, and (2) optimizing with that oracle in a tractable way.

This section lays out a generic contextual stochastic optimization (CSO) framework that does exactly that. In Section 4.1, the abstract CSO problem (denoted by \mathcal{P}) is defined. Section 4.2 shows how to construct a contextual distribution oracle $\mathcal{M}(\mathbf{s})$ from partial observations. Sections 4.3 and 4.4 introduce two solution paradigms—Contextual Sample Average Approximation and Contextual Robust Optimization—which use $\mathcal{M}(\mathbf{s})$ as input. Finally, Section 4.6 maps all of the above back to the omnichannel multi-courier CSOFP introduced in Section 3.

4.1. Generic Contextual Stochastic Optimization (CSO) Problem

Problem \mathcal{P} consists of fulfilling a set of incoming requests sequentially, each of which specifies demands for a subset of products. Let \mathcal{I} be the set of products, \mathcal{V} the set of selection options (e.g., sourcing or transport modes), and $\mathcal{Z} \subseteq \mathbb{Z}_+^{|\mathcal{I}| \times |\mathcal{V}|}$ the feasible assignment set. Each request arrives with known demand quantities $\{q_i : i \in \mathcal{I}\}$ at decision time. The decision variable $\mathbf{z} = (z_{iv})_{i \in \mathcal{I}, v \in \mathcal{V}} \in \mathcal{Z}$ assigns quantity z_{iv} of product i to option v .

Let $\tilde{\mathbf{c}} = (\tilde{c}_{iv})_{i \in \mathcal{I}, v \in \mathcal{V}} \sim \mathbb{P}$ denote the random cost vector. Assume that $\tilde{\mathbf{c}}$ is element-wise positive and the cost function $g(\mathbf{z}, \tilde{\mathbf{c}})$ is piecewise linear in \mathbf{z} . Introduce, for $j = 0, 1, \dots, n$, the breakpoint vectors

$$\mathbf{b}^j = (b_{iv}^j)_{i \in \mathcal{I}, v \in \mathcal{V}}, \quad \mathbf{b}^0 < \mathbf{b}^1 < \dots < \mathbf{b}^n \quad (\text{component-wise}),$$

so that each segment is defined as

$$[\mathbf{b}^{j-1}, \mathbf{b}^j] = \{\mathbf{z} : b_{iv}^{j-1} \leq z_{iv} \leq b_{iv}^j \forall i \in \mathcal{I}, v \in \mathcal{V}\}.$$

Let $\mathbf{a}^j = (a_{iv}^j)_{i \in \mathcal{I}, v \in \mathcal{V}}$ be the marginal-cost adjustment on segment j . Then

$$g(\mathbf{z}, \tilde{\mathbf{c}}) = (\tilde{\mathbf{c}} + \mathbf{a}^j)^\top \mathbf{z} \quad \text{if } \mathbf{z} \in [\mathbf{b}^{j-1}, \mathbf{b}^j], \quad j = 1, \dots, n, \quad (7)$$

thereby capturing volume-dependent pricing behaviors.

For each request, the fulfillment decision solves the risk-neutral stochastic optimization problem

$$\min_{\mathbf{z} \in \mathcal{Z}} \mathbb{E}_{\tilde{\mathbf{c}} \sim \mathbb{P}} [g(\mathbf{z}, \tilde{\mathbf{c}})]. \quad (8)$$

The piecewise-linear cost in (7) partitions the decision space into shipment-size tiers determined by the breakpoints $\{\mathbf{b}^j\}$. Within tier j , the marginal cost is $\tilde{\mathbf{c}} + \mathbf{a}^j$, which shifts to $\tilde{\mathbf{c}} + \mathbf{a}^{j+1}$ upon entering tier $j+1$. This formulation accommodates economies of scale (declining unit costs at higher volumes), quantity discounts (step-down pricing beyond thresholds), capacity surcharges (unit-cost premiums when exceeding lower-cost bands), and other tiered-pricing schemes.

In Problem (8), the true distribution \mathbb{P} is not readily available. However, side information often exists for each product-option pair. Let \mathbf{s}_{iv} denote the covariate vector for product i under selection option v (e.g., network state, weather, current demand). All these covariate vectors are aggregated into the state vector $\mathbf{s} = (\mathbf{s}_{iv})_{i \in \mathcal{I}, v \in \mathcal{V}}$, which encompasses all contextual information available at the time of decision. The distribution \mathbb{P} is then approximated by the conditional distribution $\mathbb{P}(\tilde{\mathbf{c}} | \mathbf{s})$, yielding the Contextual Stochastic Optimization (CSO) problem

$$\min_{\mathbf{z} \in \mathcal{Z}} \mathbb{E}_{\tilde{\mathbf{c}} \sim \mathbb{P}(\tilde{\mathbf{c}} | \mathbf{s})} [g(\mathbf{z}, \tilde{\mathbf{c}})]. \quad (9)$$

Let $\tilde{\mathbf{c}}_v = (\tilde{c}_{iv})_{i \in \mathcal{I}}$ and $\mathbf{s}_v = (s_{iv})_{i \in \mathcal{I}}$ for each $v \in \mathcal{V}$. Under the assumption that, conditional on its own covariates, each component c_v is independent across options $v \in \mathcal{V}$, one has

$$\mathbb{P}(\mathbf{c} \mid \mathbf{s}) = \prod_{v \in \mathcal{V}} \mathbb{P}_v(\mathbf{c}_v \mid \mathbf{s}_v),$$

where $\mathbb{P}_v(\cdot \mid \mathbf{s}_v)$ is the contextual distribution for option v . This assumption is reasonable when each option's cost depends primarily on its own covariates. Shared features, such as weather, create similarity but do not induce direct dependence. Consequently, Problem (9) can be written as

$$\min_{\mathbf{z} \in \mathcal{Z}} \mathbb{E}_{\tilde{\mathbf{c}} \sim \prod_{v \in \mathcal{V}} \mathbb{P}_v(\mathbf{c}_v \mid \mathbf{s}_v)} [g(\mathbf{z}, \tilde{\mathbf{c}})]. \quad (10)$$

4.2. Constructing a Contextual Distribution Oracle from Observational Data

The contextual distribution $\mathbb{P}(\mathbf{c} \mid \mathbf{s})$ is also generally unknown but can often be inferred from historical observations. In many real-world COS applications (including CSOFP) however, data are observational, i.e., only the costs corresponding to decisions actually taken were recorded. As a result, the dataset available to estimate $\mathbb{P}(\mathbf{c} \mid \mathbf{s})$ takes the form $\mathbb{D} = \{(\mathbf{s}_o, \mathbf{C}_o)\}_{o=1}^{|\mathbb{D}|}$, where $\mathbf{s}_o = (s_{iv,o})_{i \in \mathcal{I}, v \in \mathcal{V}}$ and $\mathbf{C}_o = (\mathbf{c}_{v,o})_{v \in \mathcal{V}}$ collect the context and realized costs, with $\mathbf{c}_{v,o}$ observed only if option v was selected in request o .

The learning task consists in finding a full-vector forecasting oracle \mathcal{M} that approximates $\mathbb{P}(\mathbf{c} \mid \mathbf{s})$ in a supervised manner using the dataset \mathbb{D} : \mathcal{M} receives a context \mathbf{s} as input and returns a probability distribution $\mathcal{M}(\mathbf{s})$ on the cost vector $\tilde{\mathbf{c}}$. Under the conditional independence assumption from the previous section, learning $\mathbb{P}(\mathbf{c} \mid \mathbf{s})$ amounts to learning $\mathbb{P}_v(\mathbf{c}_v \mid \mathbf{s}_v)$ for each selection option v separately. Partition the full dataset \mathbb{D} into subsets $\mathbb{D}_v = \{(\mathbf{s}_{v,1}, \mathbf{c}_{v,1}), (\mathbf{s}_{v,2}, \mathbf{c}_{v,2}), \dots\}$, representing the dataset for option v . A machine learning model \mathcal{M}_v is then trained on \mathbb{D}_v to approximate each $\mathbb{P}_v(\mathbf{c}_v \mid \mathbf{s}_v)$. Assemble the oracle as the product $\mathcal{M}(\mathbf{s}) = (\mathcal{M}_v(\mathbf{s}_v))_{v \in \mathcal{V}}$, which generates joint forecasts by treating each component independently. Note that if every \mathbf{s}_v shares the same structure and dimension, a single learning architecture can serve as \mathcal{M}_v for all $v \in \mathcal{V}$, trained on the union $\cup_{v \in \mathcal{V}} \mathbb{D}_v$.

By reducing the high-dimensional joint learning task to $|\mathcal{V}|$ manageable subproblems, this decomposition turns observational data into a black-box contextual distribution oracle $\mathcal{M}(\mathbf{s})$, which will serve as the input for the solution methods developed in Section 4.3 (C-SAA) and Section 4.4 (C-RO).

4.3. Contextual Sample Average Approximation (C-SAA)

Problem (10) is approximated by generalizing the Sample Average Approximation (SAA) method (Kleywegt et al. 2002) to contextual stochastic optimization. Given a request with covariates \mathbf{s} , the Contextual Sample Average Approximation (C-SAA) proceeds in two stages:

1. Candidate generation.

- (a) Draw N_1 independent cost vector samples $\{\boldsymbol{\xi}^n\}_{n=1}^{N_1} \sim \mathcal{M}(\mathbf{s})$, where $\boldsymbol{\xi}^n = (\xi_{iv}^n)_{i \in \mathcal{I}, v \in \mathcal{V}}$.

(b) Solve

$$\mathbf{z}_i = \arg \min_{\mathbf{z} \in \mathcal{Z}} \frac{1}{N_1} \sum_{n=1}^{N_1} g(\mathbf{z}, \boldsymbol{\xi}^n), \quad i = 1, \dots, Q,$$

independently Q times to obtain candidate solutions $\{\mathbf{z}_1, \dots, \mathbf{z}_Q\}$ with sample-average objectives $\{f_1, \dots, f_Q\}$.

(c) Compute the average objective $\underline{f} = \frac{1}{Q} \sum_{i=1}^Q f_i$, which is a statistical lower bound on the true optimal value f^* because \underline{f} is an unbiased estimator of $\mathbb{E}_{\tilde{\mathbf{c}} \sim \mathbb{P}(\mathbf{c}|\mathbf{s})}[\underline{f}]$ and $\mathbb{E}_{\tilde{\mathbf{c}} \sim \mathbb{P}(\mathbf{c}|\mathbf{s})}[\underline{f}] \leq f^*$.

2. Candidate evaluation.

(a) For each \mathbf{z}_i , draw a larger set of evaluation samples $\{\boldsymbol{\xi}^n\}_{n=1}^{N_2} \sim \mathcal{M}(\mathbf{s})$, with $N_2 \gg N_1$.

(b) Compute the re-estimated objectives $\bar{f}(\mathbf{z}_i) = \frac{1}{N_2} \sum_{n=1}^{N_2} g(\mathbf{z}_i, \boldsymbol{\xi}^n)$.

(c) Each $\bar{f}(\mathbf{z}_i)$ is an upper bound on f^* since each candidate solution is feasible; the difference $\bar{f}(\mathbf{z}_i) - \underline{f}$ approximates the optimality gap.

(d) Select the candidate \mathbf{z}^* with the smallest estimated gap.

Discussion. Unlike the reweighting approach of Bertsimas and Kallus (2020), which leverages complete historical samples for each fully-observed cost vector, C-SAA relies solely on observational data (i.e., only the costs of the selected options are available). Attempting to form all possible cost vector combinations from partial observations would lead to a combinatorial explosion as $|\mathcal{V}|$ and $|\mathbb{D}|$ grow, making such method intractable in large, high-dimensional selection spaces.

4.4. Contextual Robust Optimization (C-RO)

The performance of C-SAA largely hinges on the accuracy of the estimated contextual distribution. Robust optimization provides a hedge against misspecification of the contextual distribution by guarding against worst-case scenarios, making it a viable approach for contextual stochastic optimization. Let $\mathcal{U}(\mathbf{s}) \subset \mathbb{R}^{|\mathcal{Z}| \times |\mathcal{V}|}$ represent a contextual uncertainty set for the cost vector $\tilde{\mathbf{c}}$. The Contextual Robust Optimization (C-RO) problem is

$$\min_{\mathbf{z} \in \mathcal{Z}} \max_{\boldsymbol{\xi} \in \mathcal{U}(\mathbf{s})} g(\mathbf{z}, \boldsymbol{\xi}). \quad (11)$$

Two constructions of $\mathcal{U}(\mathbf{s})$ are considered: a discrete sampling-based set $\mathcal{U}_d(\mathbf{s})$ and a budgeted interval set $\mathcal{U}_b(\mathbf{s}, B)$.

4.4.1. Contextual Discrete Uncertainty Set Problem (11) can be reformulated into a single-level problem by enumerating every possible realization of the random vector $\tilde{\mathbf{c}}$, a standard technique in robust optimization. In principle, a discrete distribution can be generated as mentioned before, by combining all combinations of the observed data points. However, this will make the problem intractable as discussed.

To retain tractability, a sampling-based discrete uncertainty set in the same spirit of C-SAA is introduced. Let $\mathcal{U}_d(\mathbf{s}) = \{\boldsymbol{\xi}^1, \dots, \boldsymbol{\xi}^N\}$ denote a collection of N deviation scenarios drawn from $\mathcal{M}(\mathbf{s})$. The robust counterpart of (11) becomes

$$\begin{aligned} \text{(C-RO-D)} \quad & \min_{\mathbf{z} \in \mathcal{Z}, t \in \mathbb{R}} \quad t \\ \text{s.t.} \quad & t \geq g(\mathbf{z}, \boldsymbol{\xi}^n), \quad n = 1, \dots, N. \end{aligned} \quad (12)$$

4.4.2. Contextual Budgeted Interval Uncertainty Set An alternative uncertainty set is the budgeted interval set $\mathcal{U}_b(\mathbf{s}, B)$ (Bertsimas and Sim 2004), which is defined by a robust budget B . This budget limits the extent to which limits how many components of the uncertain parameter $\tilde{\mathbf{c}}$ can simultaneously deviate to their upper bounds.

Rather than estimating the full joint distribution, only the conditional lower and upper quantiles at levels q_{low} and q_{up} are needed to define a $(q_{\text{low}}, q_{\text{up}})$ prediction interval for each option.

For each option $v \in \mathcal{V}$, let $\underline{\boldsymbol{\xi}}_v = (\underline{\xi}_{iv})_{i \in \mathcal{I}}$ and $\bar{\boldsymbol{\xi}}_v = (\bar{\xi}_{iv})_{i \in \mathcal{I}}$ denote the estimated conditional q_{low} - and q_{up} -quantiles extracted from $\mathcal{M}_v(\mathbf{s}_v)$:

$$\underline{\boldsymbol{\xi}}_v = \inf\{\mathbf{u} : \mathbb{P}_v(\mathbf{c}_v \leq \mathbf{u} \mid \mathbf{s}_v) \geq q_{\text{low}}\}, \quad \bar{\boldsymbol{\xi}}_v = \inf\{\mathbf{u} : \mathbb{P}_v(\mathbf{c}_v \leq \mathbf{u} \mid \mathbf{s}_v) \geq q_{\text{up}}\}.$$

Given a budget B , the budgeted interval uncertainty set is

$$\mathcal{U}_b(\mathbf{s}, B) = \left\{ \boldsymbol{\xi} : \xi_{iv} = \underline{\xi}_{iv} + \delta_{iv} (\bar{\xi}_{iv} - \underline{\xi}_{iv}), \sum_{i,v} \delta_{iv} \leq B, \delta_{iv} \in [0, 1] \right\}.$$

With a fixed \mathbf{z} , the inner maximization problem in (11) is

$$\max_{\delta_{iv}} \sum_{i,v} (\bar{\xi}_{iv} - \underline{\xi}_{iv}) z_{iv} \delta_{iv} \quad (13)$$

$$\text{s.t.} \quad \sum_{i,v} \delta_{iv} \leq B \quad (14)$$

$$\delta_{iv} \in [0, 1], \quad \forall i, v. \quad (15)$$

Let $y_j \in \{0, 1\}$ and $w_{iv}^j \geq 0$ be auxiliary variables. Denote by $\pi \geq 0$ and $\lambda_{iv} \geq 0$ the dual variables corresponding to Constraints (14) and (15), respectively. Finally, let M be a sufficiently large constant. A valid choice for the ‘‘big-M’’ constant is $M = \max_{i,v,j} \{b_{iv}^n - b_{iv}^1, b_{iv}^{n-1}, (\underline{\xi}_{iv} + a_{iv}^j) b_{iv}^n\}$. By taking the

dual of the inner maximization problem and introducing y_j and w_{iv}^j , a robust counterpart of (11) is obtained as

$$\begin{aligned}
\text{(C-RO-B)} \quad & \min_{\mathbf{z} \in \mathcal{Z}, y, w, \pi, \lambda} \left(\sum_{i,v,j} w_{iv}^j + \pi B + \sum_{i,v} \lambda_{iv} \right) \\
\text{s.t.} \quad & \pi + \lambda_{iv} \geq (\bar{\xi}_{iv} - \underline{\xi}_{iv}) z_{iv}, \quad \forall i, v \\
& z_{iv} \leq b_{iv}^j + M(1 - y_j), \quad \forall i, v, j \\
& z_{iv} \geq b_{iv}^{j-1} - M(1 - y_j), \quad \forall i, v, j \\
& w_{iv}^j \geq (\underline{\xi}_{iv} + \alpha_{iv}^j) z_{iv} - M(1 - y_j), \quad \forall i, v, j \\
& y_j \in \{0, 1\}, w_{iv}^j \geq 0, \pi \geq 0, \lambda_{iv} \geq 0.
\end{aligned} \tag{16}$$

4.5. Performance Guarantees on C-SAA & C-RO

C-SAA replaces the unknown cost distribution with Monte-Carlo samples generated by a learned contextual oracle and minimizes the resulting empirical objective. Under standard regularity conditions, the SAA objective is statistically consistent: its optimal value converges exponentially fast to the true optimum as N_1 grows (Kleywegt et al. 2002, Shapiro et al. 2021). When the oracle is well-calibrated and N_1 is large, C-SAA thus attains the smallest *expected* cost. However, it remains sensitive to distributional misspecification and finite-sample error, which can expose the solution to rare but severe tail events.

C-RO mitigates this risk by optimizing the worst-case cost over a prescribed uncertainty set. Let a feasible solution \mathbf{z} satisfy $\max_{\xi \in \mathcal{U}(\mathbf{s})} g(\mathbf{z}, \xi) \leq t$. For a discrete uncertainty set built from N samples (C-RO-D), one obtains with probability $1 - \delta$ that

$$\Pr(g(\mathbf{z}, \tilde{\mathbf{c}}) > t) \leq \epsilon$$

provided

$$N \geq 2|\mathcal{V}||\mathcal{I}| + \frac{2|\mathcal{V}||\mathcal{I}|}{\epsilon} \ln\left(\frac{2}{\epsilon}\right) + \frac{2}{\epsilon} \ln\left(\frac{1}{\delta}\right)$$

samples are drawn (Calafiore and Campi 2006, Campi and Garatti 2008, Bertsimas et al. 2021). Although this bound grows linearly in the dimension of the uncertainty $|\mathcal{V}||\mathcal{I}|$, it too can degrade under distributional misspecification. Under a budgeted-interval uncertainty set (C-RO-B), the violation probability instead satisfies

$$\Pr(g(\mathbf{z}, \tilde{\mathbf{c}}) > t) \leq \exp\left(-\frac{B^2}{2|\mathcal{V}||\mathcal{I}|}\right),$$

so that the budget parameter B directly controls the trade-off between average-case performance and robustness (Bertsimas and Sim 2004). This tunable flexibility makes C-RO-B an attractive middle ground between C-SAA and C-RO-D.

Extending these guarantees to bound worst-case regret or post-decision surprise under partial-feedback settings—where counterfactual costs are unobserved—remains an important direction for future work.

4.6. Application to the Omnichannel Multi-Courier CSOFP

The generic CSO framework applies directly to CSOFP via the following identifications:

$$\begin{aligned} \mathcal{I} &\mapsto \{\text{SKUs}\}, & \mathcal{V} &\mapsto \mathcal{K} \times \mathcal{L}, \\ z_{iv} &\mapsto z_{ik\ell}, & \mathbf{s}_v &\mapsto \mathbf{s}_{k\ell}, \\ \tilde{\mathbf{c}} = (\tilde{c}_v)_{v \in \mathcal{V}} &\mapsto \tilde{\mathbf{d}} = (\tilde{d}_{k\ell})_{k \in \mathcal{K}, \ell \in \mathcal{L}}. & \mathbb{P}_v &\mapsto \mathbb{P}_{k\ell}. \end{aligned}$$

Under the conditional independence assumption,

$$\mathbb{P}(\mathbf{d} \mid \mathbf{s}) = \prod_{k \in \mathcal{K}} \prod_{\ell \in \mathcal{L}} \mathbb{P}_{k\ell}(d_{k\ell} \mid \mathbf{s}_{k\ell}).$$

Hence CSOFP (Problem 6) can be rewritten as

$$\min_{\mathbf{z} \in \mathcal{Z}} \mathbb{E}_{\tilde{\mathbf{d}} \sim \prod_{k, \ell} \mathbb{P}_{k\ell}(d_{k\ell} \mid \mathbf{s}_{k\ell})} [g(\mathbf{z}, \tilde{\mathbf{d}})]. \quad (17)$$

To learn each marginal distribution $\mathbb{P}_{k\ell}(d_{k\ell} \mid \mathbf{s}_{k\ell})$, partition the historical dataset into

$$\mathbb{D}_{k\ell} = \{(\mathbf{s}_{k\ell, m}, d_{k\ell, m})\}_{m=1}^{M_{k\ell}},$$

and train a per-carrier model \mathcal{M}_k on $\mathbb{D}_k = \bigcup_{\ell \in \mathcal{L}} \mathbb{D}_{k\ell}$. The full contextual distribution oracle is $\mathcal{M}(\mathbf{s}) = (\mathcal{M}_k(\mathbf{s}_{k\ell}))_{k \in \mathcal{K}, \ell \in \mathcal{L}}$.

This per-carrier decomposition simplifies learning, generalizes to new locations, and outperforms a single global model according to preliminary experiments.

4.6.1. Applying C-SAA and C-RO Computing the expectation in $\mathbb{E}_{\tilde{\mathbf{d}} \sim \mathcal{M}(\mathbf{s})} [g(\mathbf{z}, \tilde{\mathbf{d}})]$ directly would require either enumerating all $C^{|\mathcal{K}| \times |\mathcal{L}|}$ deviation vectors or numerically integrating a continuous CDF—both computationally intractable. Instead, the two solution paradigms use the contextual distribution oracle $\mathcal{M}(\mathbf{s})$ as follows:

- C-SAA replaces the expectation by a sample average: draw N_1 full-vector scenarios $\{\tilde{\mathbf{d}}^n\} \sim \mathcal{M}(\mathbf{s})$ and solve

$$\min_{\mathbf{z} \in \mathcal{Z}} \frac{1}{N_1} \sum_{n=1}^{N_1} g(\mathbf{z}, \tilde{\mathbf{d}}^n).$$

- C-RO builds an uncertainty set from oracle outputs—either the discrete scenario set $\{\tilde{\mathbf{d}}^n\}_{n \in [N]}$ or a budgeted-interval set from marginal quantiles—and then solves

$$\min_{\mathbf{z} \in \mathcal{Z}} \max_{\mathbf{d} \in \mathcal{U}(\mathbf{s})} g(\mathbf{z}, \mathbf{d}).$$

Both approaches avoid the exponential support growth while remaining agnostic to the internal structure of \mathcal{M} . A full C-RO-B reformulation is provided in the Appendix.

5. Learning the Contextual Distribution of Delivery Deviations for CSOFP

Having defined in Section 4 a generic contextual distribution oracle $\mathcal{M}(\mathbf{s})$, this section describes its concrete implementation for CSOFP. It begins by selecting features to construct the covariate vector. Two classes of machine learning methods are then proposed to estimate the contextual distribution of deviations: (1) Probabilistic multi-class classification, which leverages the discrete support of deviations; and (2) Tree-based quantile regression, which directly estimates the conditional CDF and avoids quantile crossing (Salari et al. 2022).

For simplicity, the carrier index k is omitted in the notation, and the dataset for training the per-carrier model is written as $\mathbb{D} = \{(\mathbf{s}_m, d_m)\}_{m \in [M]}$.

5.1. Contextual Feature Selection

Carefully selecting contextual features is crucial for constructing informed covariates for delivery deviation predictions, as various stages in the order life cycle can contribute to deviations.

Candidate features fall into three categories:

1. *Order-level*: This includes customer location, SKU weight and dimensions, SKU type, quantities, release hour, release day, and planned lead time (i.e., the difference between the promised delivery date and the order release time). These factors can influence deviations through logistical complexity, handling requirements, and time-sensitive elements affecting the order’s processing and delivery schedule.

2. *Fulfillment center*: This includes coordinates, location type, on-hand capacity, and on-hand inventory. The geographical location and type of fulfillment center can affect the efficiency of order processing, while capacity and inventory levels determine the speed and reliability of fulfilling orders.

3. *Carrier-related*: This includes service level, promised transit time, shipping charges, and carrier zone. These factors impact the carrier ability to meet delivery deadlines, with service level and transit times directly affecting deviations, while shipping charges and zones reflect logistical challenges and potential bottlenecks.

5.2. Probabilistic Multi-Class Classification

This discrete nature allows the contextual distribution learning problem to be framed as a multi-class classification (MC-CLF) problem. Under MC-CLF, each class represents a possible delivery deviation value in number of days, and the output class probabilities correspond directly to the probability mass function of the discrete distribution. For a new sample with covariates vector \mathbf{s} , let the conditional probability of class c be $p_c(\mathbf{s}) = \mathbb{P}(d = \xi_c \mid \mathbf{s})$, with the corresponding predicted probability from MC-CLF denoted as $\hat{p}_c(\mathbf{s})$.

Multinomial logistic regression (MLR) and classification tree-based models are considered to solve MC-CLF. Specifically, MLR is a classic classifier that aims to estimate the class probabilities by maximizing the log-likelihood function, the negative of the log loss function. The log loss is defined as $-\sum_{m=1}^M \sum_{c=1}^C \mathbf{1}\{d_m = \xi_c\} \log(\hat{p}_c(\mathbf{s}_m))$. On the other hand, classification trees use a nonparametric

approach that recursively partitions the data into subsets based on feature values in a top-down manner, resulting in a tree-like model of decisions.

Let $\mathcal{R}_1, \dots, \mathcal{R}_R$ be the regions partitioned by a classification tree. Classification tree estimates

$$\hat{p}_c(\mathbf{s}) = \frac{\sum_{r=1}^R \mathbf{1}\{\mathbf{s} \in \mathcal{R}_r\} \cdot \mathbf{1}\{d = \xi_c\}}{\sum_{r=1}^R \mathbf{1}\{\mathbf{s} \in \mathcal{R}_r\}}, \quad (18)$$

To enhance predictive power, ensemble learning methods such as bagging and gradient boosting are employed, through the use of random forests (RF) and gradient boosted trees (GBT). The details for their calculation of the class probabilities are available in Appendix.

The performance of the MC-CLF models are evaluated by log loss and Brier score. The latter is defined as the average squared error between predicted probabilities and actual outcomes $\sum_{m=1}^M \sum_{c=1}^C (\mathbf{1}\{d_m = \xi_c\} \hat{p}_c(\mathbf{s}_m))^2$. For both metrics, lower values indicate better probabilistic prediction performance.

5.2.1. Probability Calibration Raw class-probability estimates $\hat{p}_c(\mathbf{s})$ from classifiers often exhibit mis-calibration: a predicted probability α does not correspond to an empirical frequency α (Niculescu-Mizil and Caruana 2005). *Good calibration* means that, over all samples with $\hat{p}_c(\mathbf{s}) = \alpha$, the true fraction belonging to class c is approximately α . Formally, let $f(\alpha) = \mathbb{P}(d = \xi_c \mid \hat{p}_c(\mathbf{s}) = \alpha)$ be the calibration function. Perfect calibration means $f(\alpha) = \alpha$ for all $\alpha \in [0, 1]$.

Isotonic regression (Zadrozny and Elkan 2002) learns a non-decreasing mapping $g : [0, 1] \rightarrow [0, 1]$ that best aligns raw scores to observed frequencies, preserving the rank order of \hat{p}_c . Given a calibration set $\mathbb{D}_{cal} = \{(\hat{p}_c(\mathbf{s}_m), y_{c,m})\}_{m=1}^{M_{cal}}$ with $y_{c,m} = \mathbf{1}\{d_m = \xi_c\}$, isotonic regression solves

$$\min_g \sum_{m=1}^{M_{cal}} (y_{c,m} - g(\hat{p}_c(\mathbf{s}_m)))^2 \quad \text{s.t.} \quad g(\alpha) \leq g(\alpha') \text{ whenever } \alpha \leq \alpha'.$$

The calibrated probabilities are $\tilde{p}_c(\mathbf{s}) = g(\hat{p}_c(\mathbf{s}))$. By enforcing monotonicity, isotonic calibration ensures that higher raw scores remain higher after mapping, and empirical frequencies within each score bin match the calibrated values.

In this paper, a k -fold cross-validation procedure is employed: for each fold i , the classifier is trained on its training split, raw scores are obtained on the held-out calibration split, and an isotonic regression model $g^{(i)}$ is fit to those scores. On unseen test instance with covariates \mathbf{s} , each fold's classifier and corresponding $g^{(i)}$ yield calibrated probabilities $\tilde{p}_c^{(i)}(\mathbf{s})$, which are then averaged across all k folds to produce the final estimate $\tilde{p}_c(\mathbf{s}) = \frac{1}{k} \sum_{i=1}^k \tilde{p}_c^{(i)}(\mathbf{s})$.

5.3. Tree-Based Quantile Regression

Unlike multi-class classification methods that treat each deviation value as an unordered category, quantile regression (QR) exploits the inherent ordering of deviations by framing the task as ordinal regression and directly estimating the conditional cumulative distribution function (CDF) $F(u \mid \mathbf{s}) = \mathbb{P}(d \leq u \mid \mathbf{s})$.

Standard QR models minimize, for each quantile level q , the pinball loss

$$\rho_q(d, \hat{d}) = q \max(d - \hat{d}, 0) + (1 - q) \max(\hat{d} - d, 0), \quad (19)$$

where \hat{d} denotes the model's predicted q -th quantile. Collecting these quantile estimates across q yields a stepwise approximation of the CDF. However, estimating each quantile independently can violate the ordering $\hat{d}_{(q_1)} \leq \hat{d}_{(q_2)}$ for $q_1 < q_2$, resulting in a non-monotonic—and thus invalid—CDF.

Tree-based QR methods—namely regression trees extended to CDF estimation, and their ensemble version, quantile random forests (QRF) (Meinshausen and Ridgeway 2006)—avoid this “quantile crossing” problem by extracting quantiles from the empirical distribution of training sample in each leaf region.

A regression tree partitions the covariate space into disjoint regions to minimize mean squared error (MSE). Although regression trees are often used for point forecasts (e.g., predicting the mean response in each leaf), they can be adapted for distributional forecasting by preserving all observations within each partitioned region. For a new sample with covariates \mathbf{s} , let $\mathcal{R}(\mathbf{s})$ be the leaf region into which \mathbf{s} falls. The conditional CDF of the deviation can then be approximated by the empirical distribution of the training samples in that leaf:

$$\hat{F}(u | \mathbf{s}) = \sum_{m=1}^M \frac{\mathbf{1}\{\mathbf{s}_m \in \mathcal{R}(\mathbf{s})\}}{|\{j : \mathbf{s}_j \in \mathcal{R}(\mathbf{s})\}|} \mathbf{1}\{d_m \leq u\}. \quad (20)$$

A subsequent kernel density estimation applied to $\{d_m : \mathbf{s}_m \in \mathcal{R}(\mathbf{s})\}$ can further smooth this step-function CDF (Salari et al. 2022).

QRF extends this approach by pooling the leaf-level samples across an ensemble of T trees. For each tree t , let $\mathcal{R}^{(t)}(\mathbf{s})$ be leaf region containing \mathbf{s} . The QRF estimate of the conditional CDF is

$$\hat{F}(u | \mathbf{s}) = \frac{1}{T} \sum_{t=1}^T \sum_{m=1}^M \frac{\mathbf{1}\{\mathbf{s}_m \in \mathcal{R}^{(t)}(\mathbf{s})\}}{|\{j : \mathbf{s}_j \in \mathcal{R}^{(t)}(\mathbf{s})\}|} \mathbf{1}\{d_m \leq u\}. \quad (21)$$

Because this procedure pools ordered observations directly, it naturally preserves the ordinal support and never produces crossing quantiles.

To measure the distributional forecasting performance, the paper uses two metrics—the Continuous Ranked Probability Score (CRPS) and pinball loss. CRPS evaluates the closeness of the estimated CDF \hat{F} given covariates \mathbf{s} to the observed ground truth value d

$$\text{CRPS}(\hat{F}, d, \mathbf{s}) = \int_{-\infty}^{\infty} (\hat{F}(u | \mathbf{s}) - \mathbf{1}\{u \geq d\})^2 du. \quad (22)$$

Let ξ and ξ' be two independent random variables with distribution $\hat{F}(u | \mathbf{s})$. The CRPS can alternatively be expressed as

$$\text{CRPS}(\hat{F}, d, \mathbf{s}) = \mathbb{E}(|\xi - d|) - \frac{1}{2} \mathbb{E}(|\xi - \xi'|). \quad (23)$$

This equation allows for an approximation of CRPS by sampling from $\hat{F}(u | \mathbf{s})$. Pinball loss measures the accuracy of quantile predictions by penalizing errors asymmetrically, depending on whether the predictions are overestimates or underestimates.

6. Case Study

This section presents computational results that demonstrate the potential of the proposed CSO framework when evaluated on real-world industrial instances.

6.1. Data Overview

The industrial partner provides a month-long dataset in 2023, covering more than 1 million online orders for home delivery and over 20,000 unique SKUs. Each order can be sourced from roughly 250 to 1,000 possible fulfillment centers across the company’s network and shipped via one of 10 to 30 distinct carriers.

The target variable in the machine learning problem, delivery deviation, is defined as the difference between the actual delivered date and the promised delivery date. To enhance the quality of the analysis, order lines with extreme deviations were excluded—specifically, those with absolute values greater than 10 days. Such outliers often reflect exceptional circumstances, including returns to sender, lost shipments, or atypical business orders, which can introduce noise and bias into the model.

6.2. Evaluation of Contextual Distributional Learning of Delivery Deviations

This section evaluates the contextual distributional learning models presented in Section 5 for the case study.

6.2.1. Machine Learning Model Settings For the evaluation of the learning models, the dataset was partitioned into a training set comprising orders from the first three weeks (approximately 1.3 million order lines) and a test set consisting of orders from the final week (approximately 0.4 million order lines). For multi-SKU orders, features were aggregated by retaining only those of the SKU with the highest shipping charge and quantity. The MC-CLF models were implemented using scikit-learn (Pedregosa et al. 2011) and CatBoost (Prokhorenkova et al. 2018), with probability calibration applied to the best-performing uncalibrated models based on cross-validated metrics. Quantile regression models, including regression tree and QRF, were implemented via the quantile-forest package (Johnson 2024). All hyperparameters were tuned using three-fold cross-validation in Optuna (Akiba et al. 2019): MC-CLF models were tuned to minimize log loss, whereas quantile regression models were tuned to minimize CRPS.

6.2.2. Learning Performance Analysis In Table 1, two standard metrics—log loss and Brier score—are reported to measure the accuracy of probabilistic predictions for each tuned MC-CLF model on the test set. Calibration yields a clear improvement: the calibrated classifier achieves the lowest log loss (0.965) and Brier score (0.031), down from 1.050 and 0.034 for the uncalibrated gradient-boosted tree (GBT-CLF), and substantially outperforming both the random-forest classifier (RF-CLF; 1.593, 0.054) and the simpler baselines (MLR and classification tree).

Figure 2 presents the joint predicted distributions of (a) the calibrated-CLF, (b) the QRF, and (c) the discretized regression tree, each plotted against the true empirical distribution for orders fulfilled by a representative carrier. The calibrated-CLF closely reproduces the empirical mass at zero deviation (on-time

deliveries) and tightly follows the tails corresponding to early and late deliveries. The QRF exhibits slightly greater discrepancies, particularly in the majority classes (-1 to 1), while the discretized regression tree shows the largest misalignment from the empirical distribution.

Table 1 Out-of-Sample Average Log Loss and Brier Score Across All Carriers.

Model	MLR	Classification Tree	RF-CLF	GBT-CLF	Calibrated-CLF
Log loss	1.950	2.242	1.593	1.050	0.965
Brier score	0.073	0.072	0.054	0.034	0.031

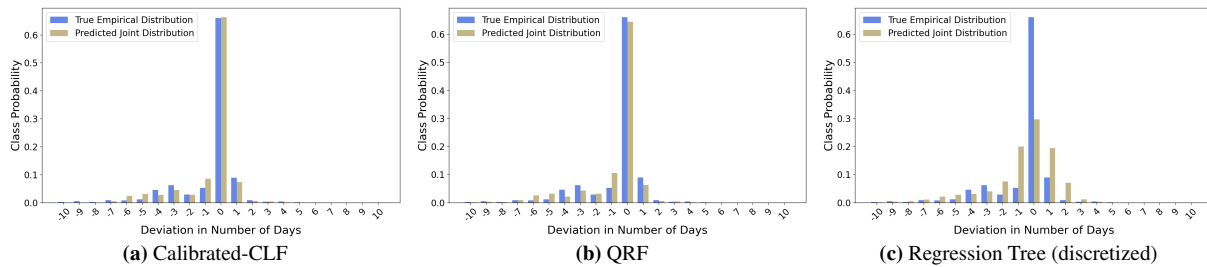


Figure 2 Out-of-Sample Comparison of the Joint Predicted Distribution and True Empirical Distribution for an Example Carrier.

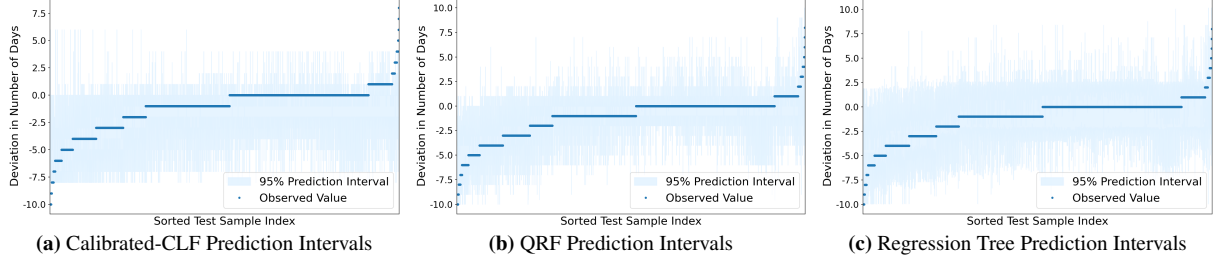
Table 2 reports pinball losses at selected quantiles and CRPS values for the tuned quantile regression and calibrated-CLF models. CRPS was approximated by drawing 1,000 samples to compute Equation (23). The calibrated-CLF model exhibit higher pinball losses than the two quantile regression models, reflecting its inherently discrete output, but nonetheless achieves the lowest CRPS overall, even though it was not directly tuned for this metric. This superior CRPS performance likely results from calibration producing sharper probability estimates, especially for the majority deviation classes.

Additionally, Figure 3 displays the 95% prediction intervals created by the three contextual distribution learning methods for an example carrier. The visualization aligns with the pinball loss results, showing that QRF generally provides the narrowest interval widths. While the intervals generated by calibrated-CLF cover most of the observed values, their coverage is less effective at the two extremes compared to the two QR methods. The inferior performance of calibrated-CLF at extreme quantiles is likely due to the discretization of the output space, which limits precision, and the cumulative probability method, which can cause jumps when selecting quantiles. In contrast, regression tree and QRF provide finer-grained predictions, leading to more accurate and narrower intervals at the extremes.

In summary, MC-CLF models excel at providing distributional forecasts, whereas QR models are better suited to generating prediction intervals on this dataset. Since QRF benefits from ensembling multiple regression trees to reduce variance and improve accuracy and consistently outperform a single regression tree, only QRF is kept for QR in the subsequent CSO evaluations.

Table 2 Out-of-Sample Average Pinball Loss and CRPS Across All Carriers.

Model	Pinball Loss				CRPS	
	$q_{0.025}$	$q_{0.05}$	$q_{0.5}$	$q_{0.95}$	$q_{0.975}$	
Calibrated-CLF	0.199	0.198	0.676	0.526	0.304	0.386
QRF	0.033	0.057	0.263	0.143	0.096	0.402
Regression Tree	0.064	0.109	0.302	0.147	0.093	0.515

**Figure 3 Sorted Observed Deviation Values versus 95% Prediction Intervals for an Example Carrier on Out-of-Sample Data.**

6.3. Baseline Models

To compare with the proposed contextual optimization models, four baseline order-fulfillment algorithms are introduced below.

1. *Pure Cost-Driven Greedy Heuristic (Greedy)*: Mimics the industrial partner’s sourcing engine by selecting, for each unit of an SKU, the carrier–location pair that minimizes the fulfillment cost. Formally, for each order it solves $\min_{\mathbf{z} \in \mathcal{Z}} \{ \sum_{i,k,\ell} (c_{\ell}^{fixed} + c_{ik\ell}^{ship}) z_{ik\ell} \}$.

2. *Empirical-SAA*: Follows the SAA framework of Section 4.3, except that each deviation sample is drawn from the overall empirical distribution P^E of the training set, without using any contextual information. For each $n \in [N_1]$ and every $(k, \ell) \in \mathcal{K} \times \mathcal{L}$, $\xi_{k\ell}^n \sim P^E$, $\boldsymbol{\xi}^n = (\xi_{k\ell}^n)_{k \in \mathcal{K}, \ell \in \mathcal{L}}$. The empirical SAA problem is $\min_{\mathbf{z} \in \mathcal{Z}} \frac{1}{N_1} \sum_{n=1}^{N_1} g(\mathbf{z}, \boldsymbol{\xi}^n)$.

3. *C-Empirical-SAA*: A slightly smarter SAA baseline that maintains separate empirical distributions P_k^E for each carrier. For each n and (k, ℓ) , $\xi_{k\ell}^n \sim P_k^E$, $\boldsymbol{\xi}^n = (\xi_{k\ell}^n)_{k \in \mathcal{K}, \ell \in \mathcal{L}}$, and it solves the same SAA problem as above.

4. *Point Predict–Then–Optimize (PTO)*: Trains per-carrier regression models $h_k(\cdot)$ to estimate the conditional mean deviations for each $(k, \ell) \in \mathcal{K} \times \mathcal{L}$, producing the point-prediction vector $\hat{\mathbf{d}} = \{h_k(\mathbf{s}_{k\ell})\}_{k \in \mathcal{K}, \ell \in \mathcal{L}}$. It then solves the deterministic problem $\min_{\mathbf{z} \in \mathcal{Z}} g(\mathbf{z}, \hat{\mathbf{d}})$.

This method is effective only if the objective function $g(\mathbf{z}, \tilde{\mathbf{d}})$ is linear in $\tilde{\mathbf{d}}$, in which case estimating the conditional distribution simplifies to estimating the conditional mean. This is because, by linearity of expectation, $\mathbb{E}_{\tilde{\mathbf{d}} \sim \mathbb{P}(\mathbf{d}|\mathbf{s})} [g(\mathbf{z}_o, \tilde{\mathbf{d}})] = g(\mathbf{z}_o, \mathbb{E}_{\tilde{\mathbf{d}} \sim \mathbb{P}(\mathbf{d}|\mathbf{s})} [\tilde{\mathbf{d}}])$. However, $g(\mathbf{z}, \tilde{\mathbf{d}})$ is nonlinear due to asymmetric penalty costs of the deviations, hence replacing the distribution by its mean may bias the solution. For each carrier, the regression model with the lowest cross-validated mean squared error is selected (see Appendix for details).

6.4. Experimental Setting

This section outlines the computational environment, simulation framework, and parameter configurations used in the experiments.

6.4.1. Implementation Environment The optimization models in this study were implemented in Python 3.9 using Gurobi 11.0.0, with eight threads allocated to each order instance. A termination criterion of a 1% MIP gap or a 5-minute time limit was applied. All experiments were conducted on a server equipped with dual-socket Intel Xeon Gold 6226 CPUs, each featuring 24 cores running at 2.7 GHz.

6.4.2. Simulation Framework One of the difficulties in this application is that the ground truth is not available for options that were not selected. To overcome this limitation, a simulation environment was built to generate synthetic “ground truth” when an algorithm selects an option. Specifically, delivery deviations were drawn from a multinomial distribution, with probabilities estimated by fitting a fine-tuned, calibrated multi-class classification model based on orders from the last week of the dataset (testing period). Obviously, this data was not accessible to the algorithm and only used by the simulator to replicate real-world conditions. The training and calibration procedures of the simulator closely followed the methodology outlined in Section 5.2. An evaluation of the simulator is provided in Appendix.

For the following experiments, as mentioned in Section 6.2, all ML models were trained on order data from the first three weeks. Evaluation was conducted on 5,000 multi-item orders, randomly sampled from the final week. To account for variability, solution metrics were computed across 50 random realizations. *All reported metrics were normalized by setting the Greedy baseline to 1 for each random seed; true performance values were omitted to due to data confidentiality.*

6.4.3. Model Names and Parameters In the following, the C-SAA problems using samples from the contextual distribution estimates provided by the MC-CLF and QRF models are referred to as C-SAA-CLF and C-SAA-QRF, respectively. Similarly, the C-RO problems are referred to as C-RO- $\{B,D\}$ -CLF and C-RO- $\{B,D\}$ -QRF, respectively.

By default, a constant $\beta_k = 0.5$ consolidation discount factor for all $k \in \mathcal{K}$ was considered. The default penalty for early delivery γ^- was 0.1 and that for late delivery γ^+ was 10. For SAA-based methods, the default was to have $Q = 20$ independent replications each with a sample size of $N_1 = 30$. The obtained solutions were then evaluated with a default sample size of $N_2 = 300$. The default sample size used for C-RO-D was $N = 200$. As for C-RO-B, a default of 95% interval was considered. Moreover, a scaling factor $\eta \in [0, 1]$ (default of 0.5) determined the uncertainty budget in C-RO-B, defined as $B = \eta |\mathcal{K}| |\mathcal{L}|$.

6.5. Overall Results

Table 3 reports the normalized average and worst-case objective values across 50 random seeds and all order instances. Based on these results, the following observations are drawn.

Average Performance The C-SAA variants and C-RO-B-CLF method lead to more reduction in the expected objective than other methods. C-SAA-CLF achieves the greatest reduction, with a normalized mean of 0.820 ± 0.003 (−18.0% versus Greedy), followed by C-SAA-QRF at 0.844 ± 0.003 (−15.6%) and C-RO-B-CLF at 0.842 ± 0.003 (−15.8%). By comparison, Empirical-SAA (0.962 ± 0.002) and PTO (0.878 ± 0.003) offer smaller improvements, and C-Empirical-SAA (0.870 ± 0.003) performs only marginally better than PTO.

Worst-Case Performance The C-RO-D methods deliver the strongest guarantees under the worst simulated outcome: C-RO-D-CLF attains 0.779 (−22.1%), C-RO-D-QRF 0.787 (−21.3%), and C-RO-B-CLF 0.811 (−18.9%). These three methods uniformly dominate the baseline and other approaches in the worst-case metric.

Overall, the C-SAA approaches excel in minimizing the expected objective, while the C-RO-D variants excel in worst-case robustness. Notably, C-RO-B-CLF strikes a strong balance between average efficiency and tail-risk protection.

Table 3 Average and Worst-Case Realized Objective Values Across Different Order Fulfillment Methods.

Method	Average Objective (95% CI)	Worst-Case Objective
Greedy	1.000 ± 0.000	1.000
PTO	0.878 ± 0.003	0.919
Empirical-SAA	0.962 ± 0.002	1.049
C-Empirical-SAA	0.870 ± 0.003	0.896
C-SAA-CLF	0.820 ± 0.003	0.823
C-SAA-QRF	0.844 ± 0.003	0.842
C-RO-B-CLF	0.842 ± 0.003	0.811
C-RO-B-QRF	0.861 ± 0.003	0.824
C-RO-D-CLF	0.928 ± 0.003	0.779
C-RO-D-QRF	0.914 ± 0.003	0.787

Note: Top 3 methods for each metric are highlighted in bold.

6.6. Effectiveness of C-SAA

This section further compares the performance of the C-SAA methods with the two Empirical-SAA baselines and the PTO.

6.6.1. Value of Contextual Information To facilitate a closer examination of the performance of the SAA-based models, Figure 4 shows the impact of varying sample sizes (N_1). On the one hand, larger sample sizes should provide a more accurate approximation of the expected value in Problem (6), assuming the delivery deviation distributions were well-estimated. On the other hand, it is important to maintain a reasonably small sample size to ensure computational efficiency. For both C-SAA methods, the effect of increasing sample sizes is obvious. The average objectives are reduced from 0.85 to 0.82 for C-SAA-CLF and 0.88 to 0.84 for C-SAA-QRF, indicating their increasing alignment with the true risk-neutral objective

function. This improvement is particularly evident in their enhanced effectiveness at avoiding cumulative lateness, defined to be the total number of late delivery days across all units in the orders. The cumulative lateness decreases by 14% for C-SAA-CLF and by 12% for C-SAA-QRF.

In contrast, both Empirical-SAA and C-Empirical-SAA struggles to improve there performance in both the average realized objective value and the cumulative lateness as the sample size grows. This is because relying solely on the empirical distribution fails to capture the variability in delivery deviation distributions, which may depend on contextual information specific to each order. A biased distributional forecasts thus guide the model wrongly to create solutions with inferior quality. Based on these observations, both contextual distributional forecasting methods proposed in the paper are successful in this application, demonstrating a stronger performance compared to using empirical distribution for delivery deviation forecasting. In summary, the value of contextual information is particularly important in order fulfillment decision-making, where the uncertainty of delivery deviation can vary drastically across different states of the environment.

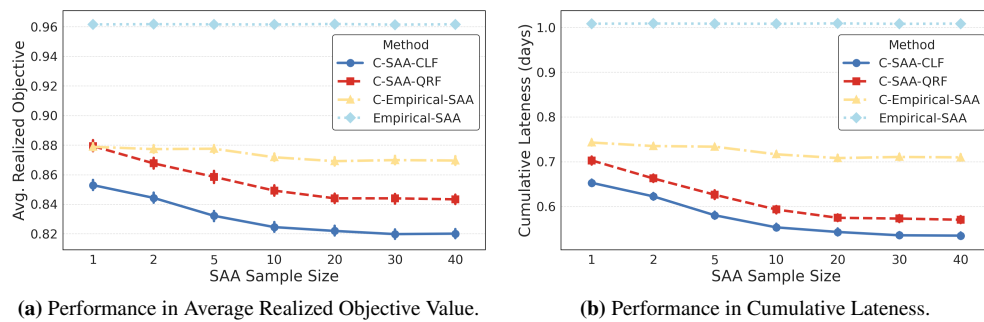


Figure 4 C-SAA vs. Empirical SAA Across Different Sample Sizes.

6.6.2. Value of Distributional Forecasts This section examines the advantage of employing distributional forecasting models over the simpler and more common point prediction model within the CSO framework. As supported by theory, simply using the conditional mean estimate of deviations to replace the expected value in CSOFP can introduce bias when approximating the true objective value, thus degrading solution quality. Figure 5 confirms that, under changing γ^+ , CSO methods with distributional estimator (C-SAA-CLF and C-SAA-QRF) consistently outperform PTO in both average realized objective value (Figure 5a) and cumulative lateness (Figure 5b). In fact, the performance differences become more pronounced as late delivery penalty (γ^+) increases.

When γ^+ raises from 2.5 to 40, PTO achieves only a 7% reduction in cumulative lateness, whereas C-SAA-CLF and C-SAA-QRF realize reductions of approximately 22% and 20%, respectively. These results demonstrate that distributional forecasting not only enables lower overall lateness but also leverages higher penalties more effectively, yielding a sharper decline in average objective and making C-SAA particularly well suited to settings where delivery timeliness is critical.

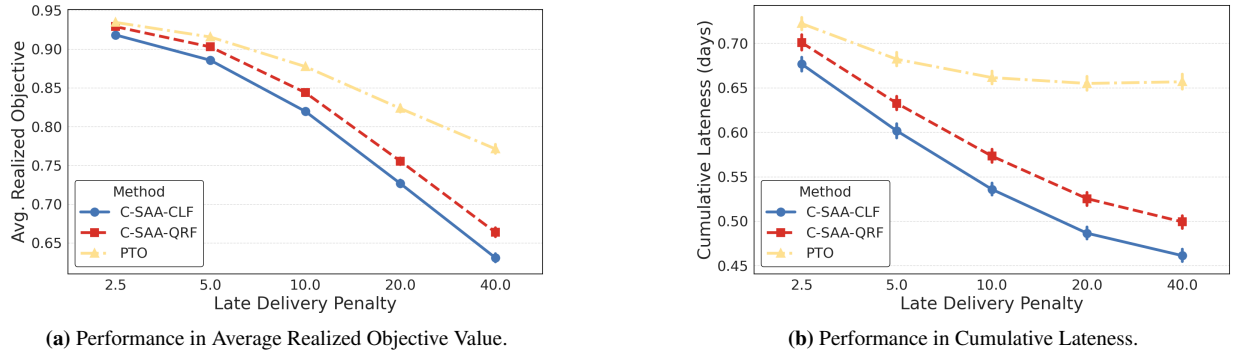


Figure 5 C-SAA vs. PTO Across Different Late Delivery Penalties.

6.7. Cost of Robustness

To quantify the trade-off between robustness and efficiency, C-RO-B-CLF and C-RO-D-CLF were compared with C-SAA-CLF as the late-delivery penalty (γ^+) increases (Figure 6).

As depicted in Figure 6a, at $\gamma^+ = 2.5$, average objectives are approximately 0.92 for C-SAA-CLF, 0.95 for C-RO-B-CLF, and 1.00 for C-RO-D-CLF. As γ^+ rises to 40, these values decline in parallel—C-SAA-CLF to 0.63, C-RO-B-CLF to 0.67, and C-RO-D-CLF to 0.73. Throughout this range, C-SAA-CLF consistently achieves the lowest average objective, followed by C-RO-B-CLF and then C-RO-D-CLF.

Worst-case objectives (Figure 6b) underscore the robustness of the C-RO methods: C-RO-D-CLF consistently yields the strongest tail protection, dropping from 0.88 at $\gamma^+ = 2.5$ to 0.72 at $\gamma^+ = 40$. C-RO-B-CLF falls from 0.885 to 0.775, while C-SAA-CLF declines more steeply from 0.925 to 0.73. Notably, at $\gamma^+ = 40$, C-SAA-CLF nearly matches C-RO-D-CLF, demonstrating that C-SAA can approach robust performance under extreme penalty scenarios.

This robustness manifests in cumulative lateness (Figure 6c). Both C-RO variants tightly control lateness with minimal sensitivity to γ^+ , whereas C-SAA-CLF's lateness drops substantially from 0.67 at $\gamma^+ = 2.5$ to 0.46 at $\gamma^+ = 40$. These robustness gains incur higher expected fulfillment costs (Figure 6d). C-RO-D-CLF's average cost increases from 1.07 to 1.20, and C-RO-B-CLF's from 1.01 to 1.05, and C-SAA-CLF from 0.96 to 1.05. Thus, while all methods incur higher costs under stricter penalties, C-RO-B-CLF exhibits the smallest relative cost increase, C-SAA-CLF and C-RO-D-CLF have more aggressive increases in costs due to more conservative decisions.

A final strategic consideration lies in selecting γ^+ to reflect firm priorities. Lower γ^+ emphasizes immediate cost savings—maximizing short-term profits—whereas higher γ^+ prioritizes on-time delivery, fostering customer satisfaction, loyalty, and long-term value. The CSOFP framework encodes this trade-off directly via γ^+ ; robust formulations (C-RO-B-CLF and C-RO-D-CLF) further reduce the need for precise γ^+ tuning by delivering stable, worst-case performance across penalty levels, while C-SAA-CLF can leverage high γ^+ most aggressively when strict timeliness is paramount.

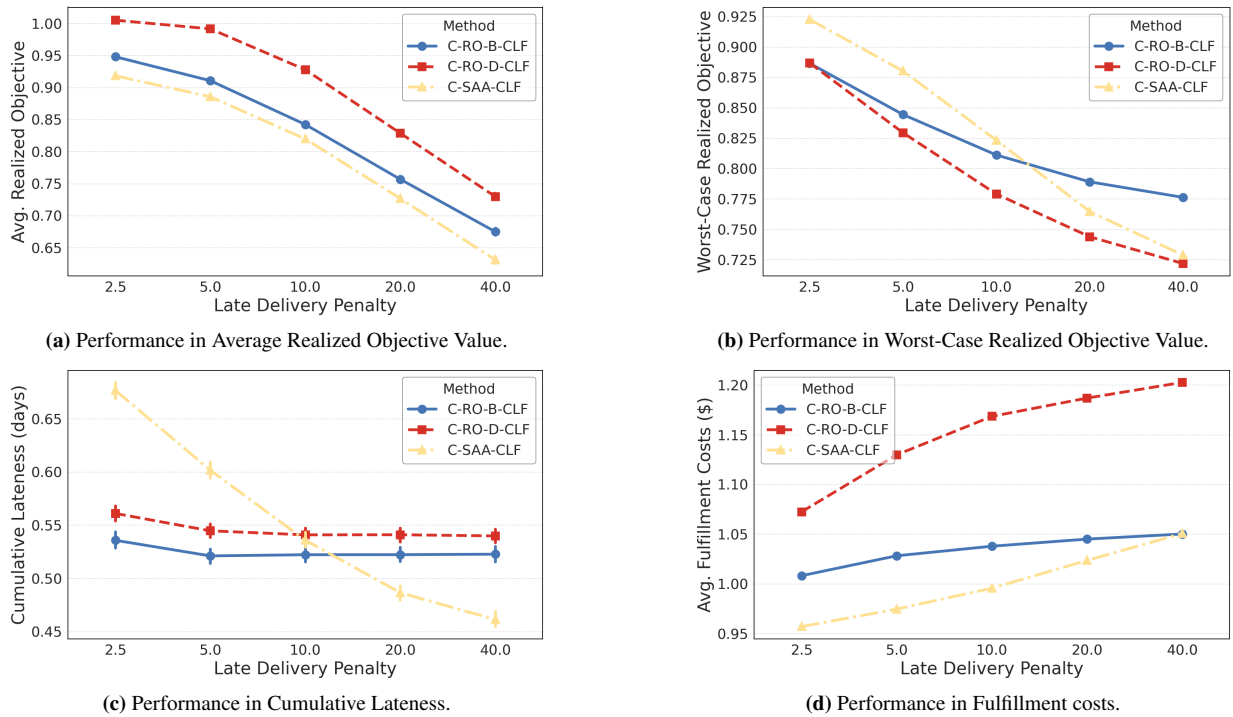


Figure 6 C-RO vs. C-SAA Across Different Late Delivery Penalties.

6.7.1. Flexibility of C-RO-B The C-RO models effectively hedge against worst-case delivery deviations and potential misspecifications in the prediction models. However, this robustness incurs more conservative decisions and higher fulfillment costs. The C-RO-B variants retain the distribution-free guarantees while introducing two tuning parameters—prediction-interval coverage and robust uncertainty budget—that directly control conservativeness. Lower coverage levels and smaller budgets yield less conservative, more cost-efficient solutions (at the expense of risk protection), whereas higher values emphasize hedging against extreme deviations by sacrificing average performance.

Figures 7 and 8 summarize how these parameters affect solution quality under both C-RO-B-CLF and C-RO-B-QRF. As the prediction interval coverage increases from 70% to 90%. In Figure 7a, increasing coverage from 70% to 90% reduces the average objective to about 0.84 (C-RO-B-CLF) and 0.86 (C-RO-B-QRF), an approximately 4% improvement relative to 70% coverage. This is consistent with the concurrent decline in cumulative lateness shown in Figure 7c. However, pushing coverage beyond 95% reverses this trend: at 99% coverage the average objective rises sharply due to the cost of extreme conservatism and, for C-RO-B-CLF, degraded prediction accuracy (reflected in a spike in lateness). By contrast, C-RO-B-QRF continues to reduce lateness at 99%, illustrating its superior tail modeling. In terms of worst-case performance (Figure 7b), both methods improve with coverage, but C-RO-B-CLF plateaus after 95%, whereas C-RO-B-QRF continues to improve at 99%.

The effect of the robust budget, controlled by the scaling factor η , appears in Figure 8. Increasing η from zero to 0.01 leads to a steep drop in the average objective for both methods (Figure 8a). Both method reach

their minimum values at $\eta = 0.01$. At the same time, the worst-case objective follows a similar pattern (Figure 8b): it falls sharply up to $\eta = 0.1$, then edges back up for both methods as the budget grows. This trend is also seen in cumulative lateness, which drops dramatically until $\eta = 0.1$ and then levels off (Figure 8c). Together, these trends show that moderate budgets capture most of the gains in both average and worst case performance, while further increases deliver diminishing returns.

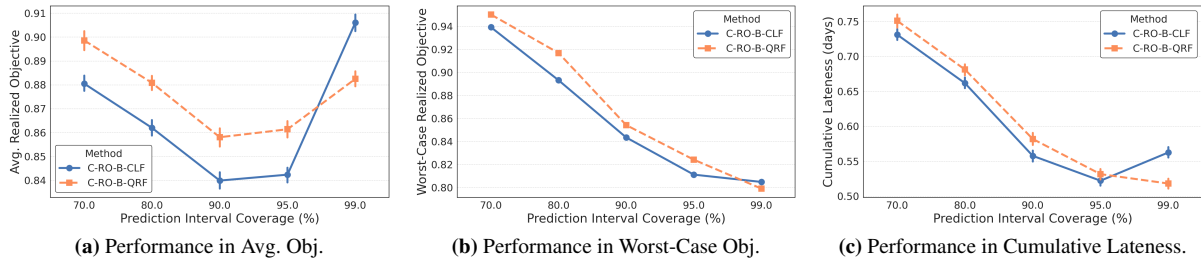


Figure 7 Performance of C-RO-B Across Different Prediction Interval Coverages.

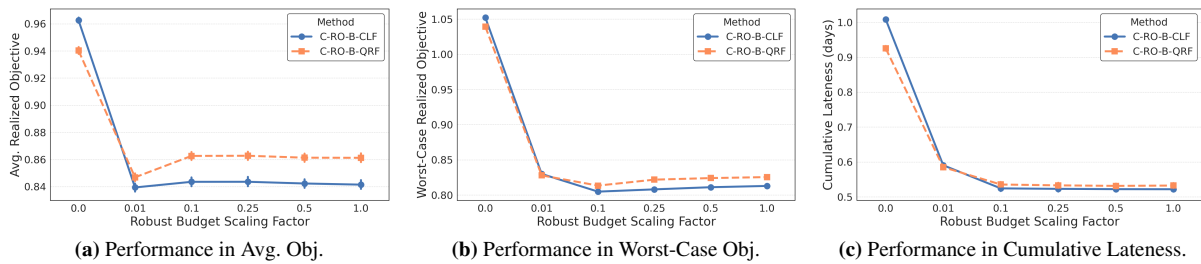


Figure 8 Performance of C-RO-B Across Different Robust Uncertainty Budgets.

6.8. Impact of Consolidation Factor

This section provides a discussion on the impact of item consolidation. CSOFP relies on the coefficients β_k to control the incentive to batch items. The industrial partner does not know the exact percentage of discount to be offered for item consolidation, which may depend on a variety of convoluted factors. Therefore, this section performs sensitivity analysis on a range of possible discount factors (from 0.1 to 0.7).

Figure 9 compares the performance of three leading methods—C-SAA-CLF, C-RO-B-CLF, and C-RO-D-CLF across average and worst-case realized objective, fulfillment cost, and consolidation level. Consolidation level is defined as the percentage of units batched (sourced and shipped by the same location-carrier pair) in each order.

As shown in Figure 9a, deeper discounts lead each method to exploit batching incentives more aggressively. C-SAA-CLF consistently attains the lowest average objective across all discount factors, declining from approximately 0.875 at $\beta = 0.1$ to about 0.785 at $\beta = 0.7$. C-RO-B-CLF follows closely, from 0.895 down to 0.805, while C-RO-D-CLF remains the most conservative, decreasing from 0.955 to 0.905.

The worst-case objective exhibits a more differentiating pattern (Figure 9a). Both C-RO-D-CLF and C-RO-B-CLF are less susceptible to change in the discount, whereas C-SAA-CLF starts at 0.842 and falls to 0.802 under high discounts.

As expected, all three methods exhibit lower average objective values due to lower fulfillment costs as the discount factor increases (see Figure 9c). This aligns with the intuition that higher discounts encourage more cost-efficient fulfillment strategies. The relative decrease in fulfillment costs across the methods can be attributed to their higher consolidation levels as the discount factor increases, as shown in Figure 9d. Notably, C-SAA-CLF responds most sharply, with its consolidation rate rising the most rapidly as the discount grows, which is consistent with its pronounced improvement in worst-case objective performance.

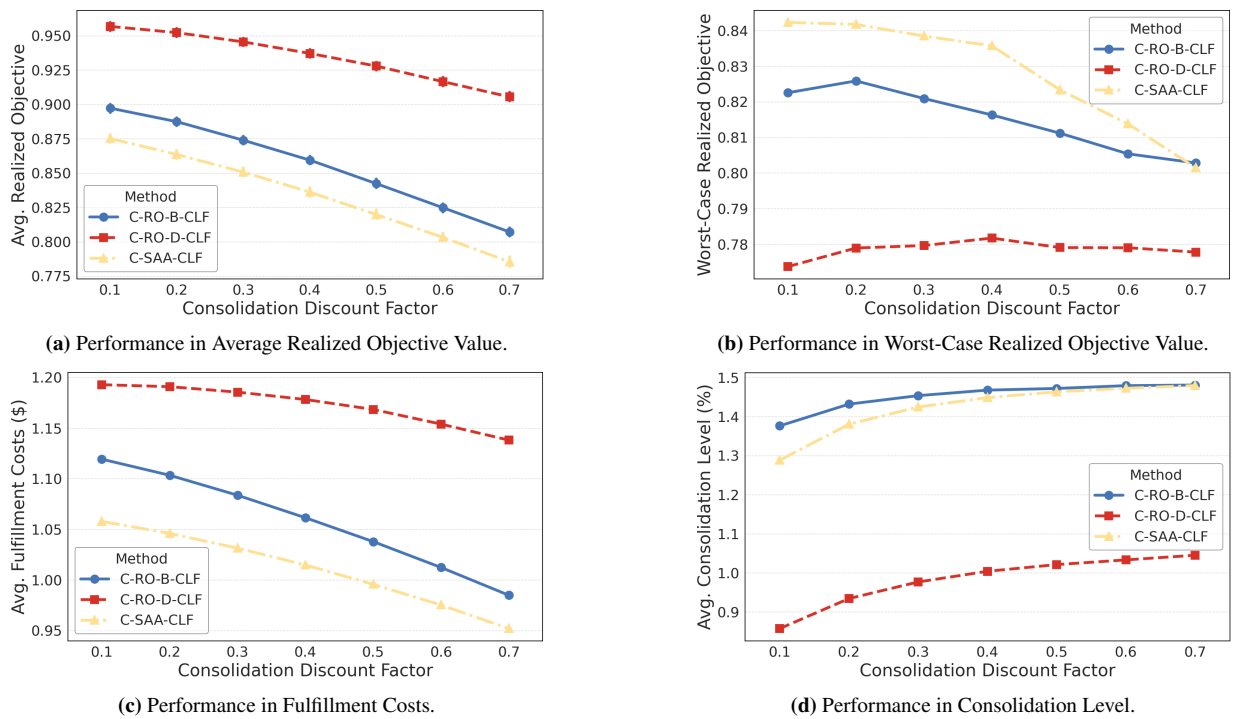


Figure 9 Performance of CSO Methods Across Different Consolidation Discount Factors.

6.9. Perturbation Analysis under Varying Simulation Environments

To assess the robustness of the proposed CSO methods, this section evaluates performance under varying simulation environments by introducing systematic perturbations to the simulated delivery time deviation distributions. These perturbations represent moderate to adversarial divergence from the test distribution, providing insight into the methods' stability under distributional shifts.

Two types of perturbations are considered: random uniform noise and delay-specific bias applied to the simulation probability distributions.

Random Uniform Noise Perturbation Let the original simulation distribution for each test instance be denoted by $P^{sim} = \{p_i\}_{i=1}^C$. For each class $i \in [C]$, a random noise term $\delta_i \sim \mathcal{U}(-\epsilon, \epsilon)$ is added to the probability p_i , resulting in: $\tilde{p}_i = p_i + \delta_i$. Negative values are clipped: $\tilde{p}_i = \max(\tilde{p}_i, 0)$, and the resulting vector is normalized to form a valid probability distribution: $\tilde{p}_i = \tilde{p}_i / \sum_j \tilde{p}_j$.

Figure 10 reports the average and worst-case realized objectives as the noise level ϵ increases. In the average case (Figure 10a), both C-RO variants degrade more gradually than C-SAA, with C-RO-B-CLF becoming the top performer beyond $\epsilon = 10$. In the worst-case scenario (Figure 10b), while all methods experience performance degrade, the ranking remains unchanged: C-RO-D achieves the lowest realized objective, followed by C-RO-B, and then C-SAA. These results indicate the superior robustness of the C-RO methods under uniform noise.

Delay-Specific Bias Perturbation Define the set of late-delay classes $C_{late} = \{i : \xi_i > 0\}$. A multiplicative bias η is applied to those classes: $\tilde{p}_i = p_i \cdot (1 + \eta)$. The probabilities for classes not in C_{late} remain unchanged. The resulting vector is clipped to the interval $[0, 1]$: $\tilde{p}_i = \max(\min(\tilde{p}_i, 1), 0)$, followed by normalization.

Figure 11 shows performance metrics for bias levels up to 250%. In the average case (Figure 11a), all CSO methods demonstrate improved performance relative to the Greedy baseline, which deteriorates rapidly. This trend is evidenced by the overall decrease in normalized objective values as the bias parameter η increases. Notably, C-RO-B overtakes C-SAA once η exceeds 150%, highlighting its robustness under adversarial delay distortions. In the worst-case objective (Figure 11b), C-RO-D consistently achieves the best performance, followed by C-RO-B-CLF. Overall, the C-RO methods exhibit lower variability in performance compared to C-SAA, indicating enhanced stability under adversarial delay conditions.

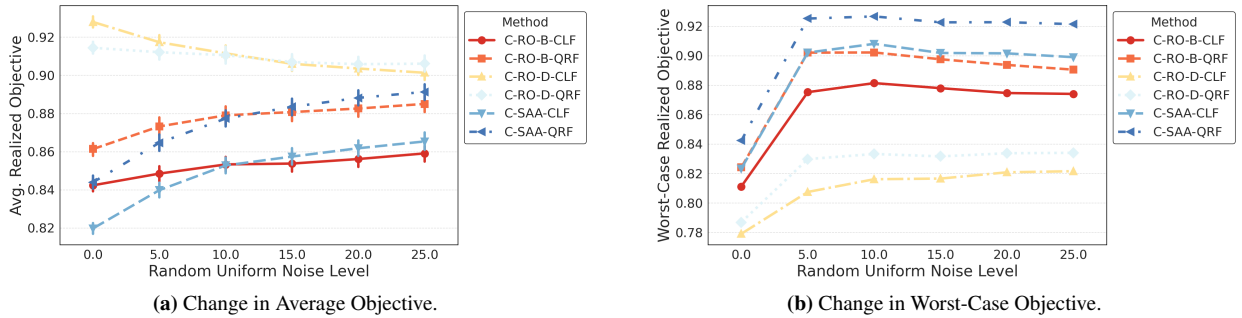


Figure 10 Performance Across Different Random Uniform Noise Perturbations.

6.10. Computational Scalability of the CSO Methods

The computational scalability of the proposed framework was evaluated by measuring both the change in computation time (model construction + solve time) and solution quality as instance size grows. Each CSOFP instance is characterized by the number of items $|Z|$ and the number of location–carrier pairs (fulfillment options) $|\mathcal{K}| \times |\mathcal{L}|$. In practice, the eligibility constraint (Constraint (3)) is used to prune infeasible

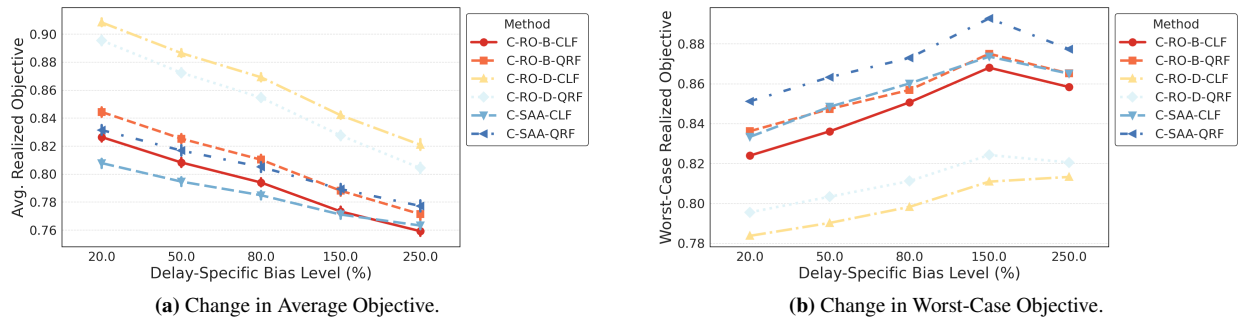


Figure 11 Performance Across Different Delay-Specific Bias Perturbations.

location–carrier pairs in advance. Then, $(\mathcal{K}', \mathcal{L}') = \{(k, \ell) \in \mathcal{K} \times \mathcal{L} \mid \exists i \in \mathcal{I} : e_{ik\ell} = 1\}$ yields the final set of eligible fulfillment options and thus the effective problem size.

Figure 12a shows computation time as the number of eligible fulfillment options increases. Only the MC-CLF variants of C-RO and C-SAA are displayed, since their QRF counterparts exhibit nearly identical runtimes. All three methods achieve optimality on every instance within minutes, confirming their practical applicability. In particular, C-RO-B solves most instances in under one second (never exceeding three seconds), and C-RO-D solves most in under ten seconds.

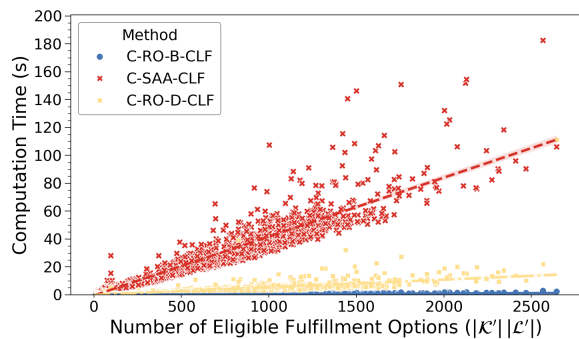
These timing differences reflect each method’s formulation. Compared to the nominal problem, the robust counterpart in C-RO-B introduces only continuous variables whose count grows linearly with $|\mathcal{K}'|$ and $|\mathcal{L}'|$. By contrast, C-RO-D adds N extra constraints from sampling, and C-SAA requires solving Q independent problems whose objective function complexity scales with the sample size N_1 . Parallel computation of the Q subproblems can further reduce C-SAA’s runtime.

Since single-item orders account for the majority of order volume, multi-item orders (what the methods are designed for) can be routed to a dedicated sourcing engine without disrupting standard operations. Under normal load, any of the three methods may be applied; under peak loads—such as holiday surges—C-RO-B is recommended to preserve fast solve times while maintaining high solution quality. Concurrent batches of orders can be processed in parallel when computational resources permit.

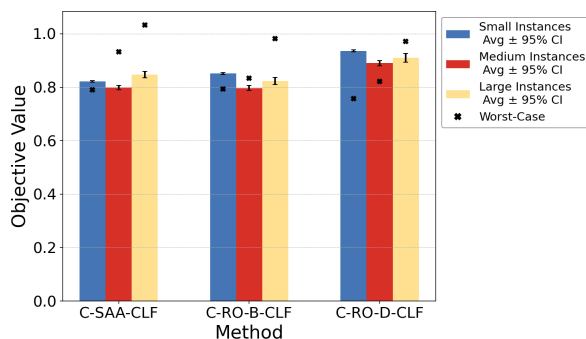
Figure 12b reports average and worst-case objective values for small (≤ 400 eligible options), medium (≤ 1000 eligible options), and large (≤ 3000 eligible options) instances. Average performance remains uniformly high across all size categories, whereas worst-case deviations grow with instance size. Collectively, these results demonstrate near-linear scalability in computation time, consistent high solution quality, and robustness across problem sizes, providing empirical evidence of the framework’s practical scalability.

6.11. Managerial and Operational Implications

The proposed fulfillment framework offers actionable guidance for practitioners seeking to align sourcing strategies with demand variability, service-level requirements, and computational constraints. Depending on the operating context, different methods are preferable. When demand is stable and the goal is to minimize



(a) Change in the Computation Time vs. the Number of Eligible Fulfillment Options.



(b) Objective Value by Instance Categories.

Figure 12 Computational Scalability Analysis.

average fulfillment cost, C-SAA-CLF provides the most cost-effective solution. Under moderate runtime constraints, C-RO-B-CLF offers a balanced trade-off between efficiency and robustness. In contrast, during high-stakes periods such as holiday promotions or flash sales—where the cost of service-level violations is high—C-RO-D-CLF and C-RO-B-QRF (with 99% coverage) are better suited to mitigate tail risks and ensure reliability. This scenario-driven approach allows e-commerce platforms to dynamically adapt fulfillment strategies to shifting conditions while leveraging a unified optimization infrastructure. As retailers increasingly face variable demand patterns and rising customer expectations, the ability to flexibly match fulfillment strategy to context becomes a key operational advantage.

Empirical evaluations indicate that the proposed methods can reduce combined fulfillment cost and delivery-timeliness penalties by an average of up to 18% per order under the default settings. To illustrate the potential impact, consider a retailer operating at a scale comparable to the industrial partner, with per-order costs ranging from \$5 to \$30 and monthly volumes of 0.1 to 1 million multi-item orders. Under these scenarios, the corresponding annual savings could range from several million to tens of millions of dollars. Moreover, this framework can be readily extended to single-item orders, which could yield further savings with minimal incremental investment.

7. Conclusion

This paper introduces a generic contextual stochastic optimization (CSO) framework for data-driven decision making when only observational data—hence missing counterfactual costs—are available. The framework is deliberately modular. First, any algorithm capable of returning a full predictive distribution can serve as the *contextual distribution oracle*. In the empirical study, calibrated multi-class classifiers and tree-based quantile-regression forests were selected to capture the discrete, ordered nature of delivery-time deviations. Second, the oracle feeds directly into two tractable optimization engines: (i) a *Contextual Sample-Average Approximation* (C-SAA) for risk-neutral objectives and (ii) a *Contextual Robust Optimization* (C-RO) formulation for risk-averse objectives. Because the learning and optimization layers communicate only through the oracle, the template can be readily translated to other operations-management settings.

When applied to an omnichannel, multi-courier order-fulfillment problem, the CSO framework reduced the combined cost–service objective by up 18% on average and up to 22% in the simulated worst case on an industry-scale data set, implying annual savings from several to tens of millions of dollars. This framework allows practitioners to tune robustness—raising it during promotional peaks and relaxing it in steadier periods—while still exploiting item-consolidation discounts and heterogeneous carrier performance in the dynamic e-commerce landscape.

While the paper delivers an end-to-end prototype with demonstrable impact, several avenues remain open:

- Performance guarantees under partial feedback: Establish theoretical performance guarantees, such as worst-case regret and post-decision surprise, for CSO methods under the partial-feedback setting. Linking causal-inference techniques with SAA and RO theory can be a promising direction, thereby quantifying the value of additional data when counterfactual costs remain unobserved.
- Hybrid distributional forecasters: Develop distributional models that fuse the calibration strength of classification with the sharp tails of quantile regression, yielding tighter and more informative uncertainty sets.
- End-to-end predict-then-prescribe learning for observational data: Incorporate downstream optimization loss directly into training, extending recent “integrated predict-then-optimize” approaches (Qi et al. 2021, Elmachtoub and Grigas 2022) to settings where data are purely observational.
- Multi-period, inventory-aware CSO: Extend the framework to jointly optimize sourcing, shipping, and stocking over rolling horizons, capturing inventory replenishment spillovers and elevate the model from a myopic to a long-term strategic planning tool.

References

- Acimovic J, Farias VF (2019) The fulfillment-optimization problem. *Operations Research & Management Science in the age of analytics*, 218–237 (INFORMS).
- Acimovic J, Graves SC (2015) Making better fulfillment decisions on the fly in an online retail environment. *Manufacturing & Service Operations Management* 17(1):34–51.
- Akiba T, Sano S, Yanase T, Ohta T, Koyama M (2019) Optuna: A next-generation hyperparameter optimization framework. *Proceedings of the 25th ACM SIGKDD international conference on knowledge discovery & data mining*, 2623–2631.
- Bayram V, Baloch G, Gzara F, Elhedhli S (2022) Optimal order batching in warehouse management: A data-driven robust approach. *INFORMS Journal on Optimization* 4(3):278–303.
- Behrendt A, Savelsbergh M, Wang H (2023) A prescriptive machine learning method for courier scheduling on crowd-sourced delivery platforms. *Transportation Science* 57(4):889–907.

- Bertsimas D, Den Hertog D, Pauphilet J (2021) Probabilistic guarantees in robust optimization. *SIAM Journal on Optimization* 31(4):2893–2920.
- Bertsimas D, Dunn J, Mundru N (2019) Optimal prescriptive trees. *INFORMS Journal on Optimization* 1(2):164–183.
- Bertsimas D, Kallus N (2020) From predictive to prescriptive analytics. *Management Science* 66(3):1025–1044.
- Bertsimas D, Kallus N, Hussain A (2016) Inventory management in the era of big data. *Production and operations management* 25(12):2006–2009, URL <http://dx.doi.org/10.1111/poms.12637>.
- Bertsimas D, Sim M (2004) The price of robustness. *Operations research* 52(1):35–53.
- Breiman L (2001) Random forests. *Machine learning* 45:5–32.
- Calafiore GC, Campi MC (2006) The scenario approach to robust control design. *IEEE Transactions on automatic control* 51(5):742–753.
- Campi MC, Garatti S (2008) The exact feasibility of randomized solutions of uncertain convex programs. *SIAM Journal on Optimization* 19(3):1211–1230.
- Chen S, Yan Z, Lim YF (2024) Managing the personalized Order-Holding problem in online retailing. *Manufacturing & Service Operations Management* 26(1):47–65, URL <http://dx.doi.org/10.1287/msom.2023.1201>.
- Chen T, Guestrin C (2016) XGBoost: A scalable tree boosting system. *Proceedings of the 22nd ACM SIGKDD International Conference on Knowledge Discovery and Data Mining*, 785–794, KDD '16 (New York, NY, USA: ACM), ISBN 978-1-4503-4232-2, URL <http://dx.doi.org/10.1145/2939672.2939785>.
- Cui R, Lu Z, Sun T, Golden JM (2024) Sooner or later? promising delivery speed in online retail. *Manufacturing & Service Operations Management* 26(1):233–251.
- Das S, Ravi R, Sridhar S (2023) Order fulfillment under pick failure in omnichannel Ship-From-Store programs. *Manufacturing & service operations management* 25(2):508–523, URL <http://dx.doi.org/10.1287/msom.2022.1164>.
- Deng Y, Sen S (2022) Predictive stochastic programming. *Computational Management Science* 19(1):65–98.
- Dethlefs C, Ostermeier M, Hübner A (2022) Rapid fulfillment of online orders in omnichannel grocery retailing. *EURO journal on transportation and logistics* 11:100082, URL <http://dx.doi.org/10.1016/j.ejtl.2022.100082>.
- DeValve L, Wei Y, Wu D, Yuan R (2023) Understanding the value of fulfillment flexibility in an online retailing environment. *Manufacturing & service operations management* 25(2):391–408.
- Elmachtoub AN, Grigas P (2022) Smart “predict, then optimize”. *Management Science* 68(1):9–26.
- Fisher ML, Gallino S, Xu JJ (2019) The value of rapid delivery in omnichannel retailing. *Journal of marketing research* 56(5):732–748, URL <http://dx.doi.org/10.1177/0022243719849940>.

- Freedman L (2019) Why logistics have never been more important to online retailers' success. URL <https://www.digitalcommerce360.com/2019/09/30/why-logistics-have-never-been-more-important-to-online-retailers-success/>.
- Friedman JH (2001) Greedy function approximation: a gradient boosting machine. *Annals of statistics* 1189–1232.
- Guan H, Gillani N, Simko T, Mangat J, Van Hentenryck P (2024) Contextual stochastic optimization for school desegregation policymaking. *arXiv preprint arXiv:2408.12572* .
- Hübner AH, Kuhn H, Sternbeck MG (2013) Demand and supply chain planning in grocery retail: an operations planning framework. *International journal of retail & distribution management* 41(7):512–530, URL <http://dx.doi.org/10.1108/ijrdm-05-2013-0104>.
- Ito S, Fujimaki R (2016) Optimization beyond prediction: Prescriptive price optimization. URL <https://arxiv.org/abs/1605.05422>.
- Jasin S, Sinha A (2015) An lp-based correlated rounding scheme for multi-item ecommerce order fulfillment. *Operations Research* 63(6):1336–1351.
- Jo N, Aghaei S, Gómez A, Vayanos P (2021) Learning optimal prescriptive trees from observational data. *arXiv preprint arXiv:2108.13628* .
- Johnson RA (2024) quantile-forest: A python package for quantile regression forests. *Journal of Open Source Software* 9(93):5976, URL <http://dx.doi.org/10.21105/joss.05976>.
- Kallus N, Mao X (2023) Stochastic optimization forests. *Management Science* 69(4):1975–1994.
- Kandula S, Krishnamoorthy S, Roy D (2021) A prescriptive analytics framework for efficient e-commerce order delivery. *Decision Support Systems* 147:113584.
- Kannan R, Bayraksan G, Luedtke JR (2023) Residuals-based distributionally robust optimization with covariate information. *Mathematical Programming* 1–57.
- Kleywegt AJ, Shapiro A, Homem-de Mello T (2002) The sample average approximation method for stochastic discrete optimization. *SIAM Journal on optimization* 12(2):479–502.
- Kuhn H, Sternbeck MG (2013) Integrative retail logistics: An exploratory study. *Operations management research/Operations management research : advancing practice through research* 6(1-2):2–18, URL <http://dx.doi.org/10.1007/s12063-012-0075-9>.
- Lattimore T, Szepesvári C (2020) *Bandit algorithms* (Cambridge University Press).
- Liu S, He L, Max Shen ZJ (2021) On-time last-mile delivery: Order assignment with travel-time predictors. *Management Science* 67(7):4095–4119.
- Lundberg SM, Erion G, Chen H, DeGrave A, Prutkin JM, Nair B, Katz R, Himmelfarb J, Bansal N, Lee SI (2020) From local explanations to global understanding with explainable ai for trees. *Nature Machine Intelligence* 2(1):2522–5839.

- Ma W (2023) Order-optimal correlated rounding for fulfilling multi-item e-commerce orders. *Manufacturing & Service Operations Management* .
- Meinshausen N, Ridgeway G (2006) Quantile regression forests. *Journal of machine learning research* 7(6).
- Meller J, Taigel F, Pibernik R (2018) Prescriptive Analytics for Inventory Management: A comparison of New approaches. *Social Science Research Network* URL <http://dx.doi.org/10.2139/ssrn.3229105>.
- Mišić VV, Perakis G (2020) Data analytics in operations management: A review. *Manufacturing & Service Operations Management* 22(1):158–169.
- Mohri SS, Ghaderi H, Nassir N, Thompson RG (2023) Crowdshipping for sustainable urban logistics: A systematic review of the literature. *Transportation research. Part E, Logistics and transportation review* 178:103289, URL <http://dx.doi.org/10.1016/j.tre.2023.103289>.
- Niculescu-Mizil A, Caruana R (2005) Predicting good probabilities with supervised learning. *Proceedings of the 22nd international conference on Machine learning*, 625–632.
- Notz PM, Pibernik R (2022) Prescriptive analytics for flexible capacity management. *Management Science* 68(3):1756–1775.
- Patel YP, Rayan S, Tewari A (2024) Conformal contextual robust optimization. *International Conference on Artificial Intelligence and Statistics*, 2485–2493 (PMLR).
- Pedregosa F, Varoquaux G, Gramfort A, Michel V, Thirion B, Grisel O, Blondel M, Prettenhofer P, Weiss R, Dubourg V, Vanderplas J, Passos A, Cournapeau D, Brucher M, Perrot M, Duchesnay E (2011) Scikit-learn: Machine learning in python. *Journal of Machine Learning Research* 12:2825–2830.
- Perakis G, Sim M, Tang Q, Xiong P (2023) Robust pricing and production with information partitioning and adaptation. *Management Science* 69(3):1398–1419.
- Peršak E, Anjos MF (2023) Contextual robust optimisation with uncertainty quantification. *International Conference on Integration of Constraint Programming, Artificial Intelligence, and Operations Research*, 124–132 (Springer).
- Prokhorenkova L, Gusev G, Vorobev A, Dorogush AV, Gulin A (2018) Catboost: unbiased boosting with categorical features. *Advances in Neural Information Processing Systems* 31.
- Qi M, Grigas P, Shen ZJM (2021) Integrated conditional estimation-optimization. *arXiv preprint arXiv:2110.12351* .
- Qi M, Shen ZJ (2022) Integrating prediction/estimation and optimization with applications in operations management. *Tutorials in Operations Research: Emerging and Impactful Topics in Operations*, 36–58 (INFORMS).
- Raj G, Roy D, de Koster R, Bansal V (2024) Stochastic modeling of integrated order fulfillment processes with delivery time promise: Order picking, batching, and last-mile delivery. *European Journal of Operational Research* .
- Sadana U, Chenreddy A, Delage E, Forel A, Frejinger E, Vidal T (2024) A survey of contextual optimization methods for decision-making under uncertainty. *European Journal of Operational Research* .

- Salari N, Liu S, Shen ZJM (2022) Real-time delivery time forecasting and promising in online retailing: When will your package arrive? *Manufacturing & Service Operations Management* 24(3):1421–1436.
- Shapiro A, Dentcheva D, Ruszczyński A (2021) *Lectures on stochastic programming: modeling and theory* (SIAM).
- Sun C, Liu L, Li X (2024) Predict-then-calibrate: A new perspective of robust contextual lp. *Advances in Neural Information Processing Systems* 36.
- Tian X, Yan R, Wang S, Liu Y, Zhen L (2023) Tutorial on prescriptive analytics for logistics: What to predict and how to predict. *Electronic Research Archive* .
- Ülkü MA (2012) Dare to care: Shipment consolidation reduces not only costs, but also environmental damage. *International Journal of Production Economics* 139(2):438–446.
- US Department of Commerce (2024) QUARTERLY RETAIL E-COMMERCE SALES. URL https://www.census.gov/retail/mrts/www/data/pdf/ec_current.pdf.
- Viswanathan A (2023) Elevating the last mile: Transformative trends and customer-centric evolution in e-commerce. URL <https://www.scmr.com/article/elevating-the-last-mile-transformative-trends-in-ecommerce>, accessed: 2024-07-05.
- Wagner L, Calvo E, Amorim P (2023) Better Together! The Consumer Implications of Delivery Consolidation. *Manufacturing & Service Operations Management* 25(3):903–920, URL <http://dx.doi.org/10.1287/msom.2023.1200>.
- Wei L, Kapuscinski R, Jasin S (2021) Shipping consolidation across two warehouses with delivery deadline and expedited options for e-commerce and omni-channel retailers. *Manufacturing & Service Operations Management* 23(6):1634–1650.
- Xu PJ, Allgor R, Graves SC (2009) Benefits of reevaluating real-time order fulfillment decisions. *Manufacturing & Service Operations Management* 11(2):340–355.
- Zadrozny B, Elkan C (2002) Transforming classifier scores into accurate multiclass probability estimates. *Proceedings of the eighth ACM SIGKDD international conference on Knowledge discovery and data mining*, 694–699.
- Zehtabian S, Larsen C, Wøhlk S (2022) Estimation of the arrival time of deliveries by occasional drivers in a crowdshipping setting. *European journal of operational research* 303(2):616–632, URL <http://dx.doi.org/10.1016/j.ejor.2022.02.050>.
- Zhao Y, Wang X, Xin L (2020) Multi-Item Online Order Fulfillment: A Competitive analysis. *SSRN Electronic Journal* URL <http://dx.doi.org/10.2139/ssrn.3675117>.

Appendix

A. MILP Model Notations

Table 4 Optimization Model Nomenclature

Sets	
\mathcal{I}	Set of SKUs, indexed by i .
\mathcal{K}	Set of carriers, indexed by k .
\mathcal{L}	Set of locations, indexed by ℓ .
Parameters	
$\text{inv}_{i\ell}$	Inventory level of SKU i at location ℓ when the order is placed.
cap_{ℓ}	Available capacity at location ℓ when the order is placed.
$e_{ik\ell}$	1 if (carrier k , location ℓ) is an eligible candidate location-carrier pair for SKU i in the order and 0 otherwise.
$c_{ik\ell}^{\text{ship}}$	Per-unit shipping cost when using location ℓ and carrier k to ship SKU i .
c_{ℓ}^{fixed}	Per-unit fixed sourcing (non-parcel) cost when using location ℓ .
β_k	Discount factor for shipping multiple units using carrier k .
q_i	Quantity of SKU i in the order.
$d_{k\ell}$	Delivery time deviation when using location ℓ and carrier k .
γ^+	Constant that converts late delivery penalty into a per-unit cost.
γ^-	Constant that converts early delivery penalty into a per-unit cost.
N	A large number = $\sum_{i \in \mathcal{I}} q_i + 2$.
$M_{k\ell}$	A large number = $\sum_{i \in \mathcal{I}} c_{ik\ell}^{\text{ship}} q_i$.
Decision Variables	
$z_{ik\ell}$	Integer decision variable which measures the quantity of SKU i in the order sourced from location ℓ and shipped by carrier k .
$y_{k\ell}$	Binary decision variable which equals 1 if more than one unit is sourced from location ℓ and carrier k within the order, and equals 0 otherwise.
$w_{k\ell}$	Continuous decision variable which measures the cost to be discounted in the order using location-carrier pair (k, ℓ) .

B. Data Preprocessing

To optimize the dataset for machine learning and optimization models, several preprocessing steps were implemented to clean the data. Duplicate entries and rows with missing values were removed. Geographic coordinates were generated from the zip codes of the fulfillment centers and customer locations, with any invalid zip codes discarded in the process. The geographic distance between customer and fulfillment center locations was approximated using the Haversine formula. Additionally, the dataset was filtered to include only carriers with sufficient order history for training prediction models, resulting in a subset of carriers.

C. Descriptive Analytics and Insights

The company receives tens of thousands of home delivery online orders daily, with an average ranging from 30,000 to 70,000 orders. During peak hours, 500 to 2,000 orders may be received within a 15-minute time window. Direct information regarding which carriers are available to ship specific SKUs from particular fulfillment centers is not available in the dataset. However, heuristic rules can be derived through analyses of historical orders. The customer's location and the dimensions/weight of the SKU(s) in an order are critical factors in determining carrier suitability.

Some carriers show a more scattered distribution of customer locations, indicating limited coverage in certain states of the U.S.. Additionally, coverage is dependent on the location of the fulfillment center from which the order is shipped, as some carriers can only serve a limited range around that center. In contrast, other carriers have served locations spanning nearly the entire US. Furthermore, the upper bounds of SKU length, height, and weight in the historical data reflect the package size and weight limits of different carriers.

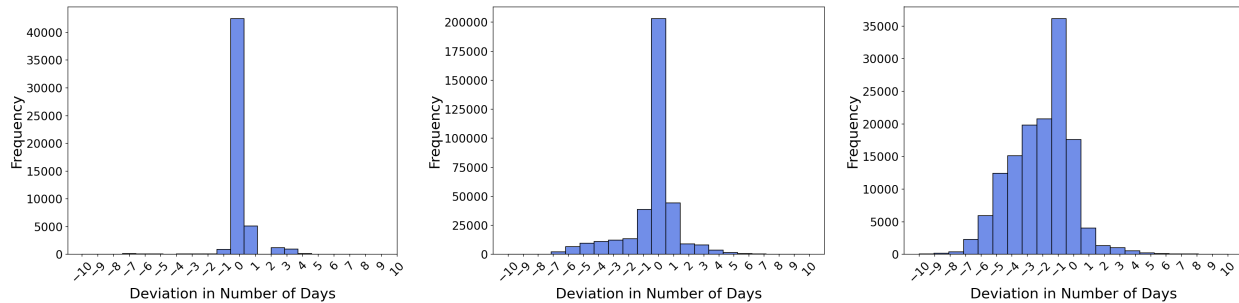


Figure 13 Delivery Deviation Distribution of Orders Shipped by Three Example Carriers.

The distribution of deviations varies significantly across carriers, as illustrated in Figure 13. For the first two carriers, the majority of orders are delivered on time. The first carrier shows nearly all on-time deliveries, with the remaining orders arriving late. The second carrier has approximately half of the orders delivered on time, with slightly more early deliveries than late ones. In contrast, orders shipped by the last carrier predominantly arrive one day early, and most deliveries arrive ahead of schedule. Given these pronounced differences, separate prediction models were developed for each carrier.

D. Feature Importance

To identify the most important features for predicting deviations, a feature importance analysis was conducted using a tree-based regression model. Two methods were examined: Mean Decrease in Impurity (MDI) and Shapley values (SHAP). MDI measures the importance of a feature by calculating the total reduction in impurity (e.g., Gini impurity or entropy) it brings when used in decision trees (Breiman 2001). SHAP values, on the other hand, provide a unified measure of feature importance based on cooperative game theory, attributing to each feature its contribution to the prediction by considering all possible feature combinations (Lundberg et al. 2020).

Figure 14 highlights the top 10 most important features evaluated, as evaluated using MDI and SHAP, for an example carrier under a tree-based regression model. For this carrier, the planned lead time (promised delivery time) emerges as the most significant factor. Additionally, order information such as the release time and SKU type, fulfillment center characteristics like on-hand capacity, and carrier-specific attributes such as promised time-in-transit and carrier zone also play important roles.

E. Linearize the Objective Function of the Order Fulfillment Problem

The nonlinear objective function $g(\mathbf{z}, \mathbf{d})$ can be linearized using auxiliary variables. Let $\mathbf{y} = (y_{k\ell})_{k \in \mathcal{K}, \ell \in \mathcal{L}} \in \{0, 1\}^{(|\mathcal{K}| |\mathcal{L}|)}$ be indicator variables, where $y_{k\ell} = 1$ indicates more than one unit is sourced from location ℓ and shipped by carrier k within the order. Additionally, let $\mathbf{w} = (w_{k\ell})_{k \in \mathcal{K}, \ell \in \mathcal{L}} \in \mathbb{R}^{(KL)^+}$ be continuous variables, where $w_{k\ell}$ represents the shipping costs to be discounted in the order using carrier-location pair (k, ℓ) .

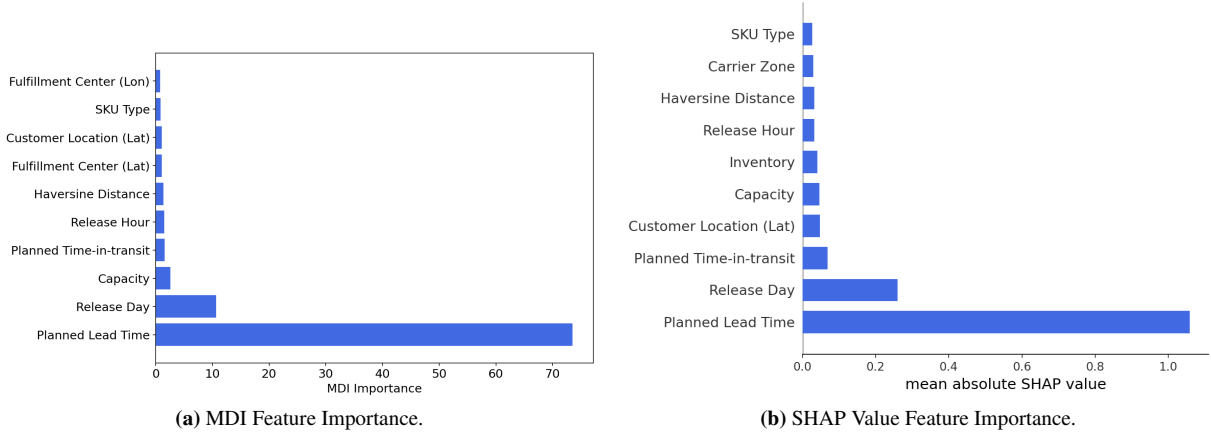


Figure 14 Top 10 Mean Regression Features for Delivery Deviation Measured by Two Feature Importance Metrics For an Example Carrier.

The linear objective function and the additional constraints for linearization are defined as follows:

$$g(\mathbf{z}, \mathbf{d}) = \left(\sum_{i \in \mathcal{I}} \sum_{k \in \mathcal{K}} \sum_{\ell \in \mathcal{L}} (c_{\ell}^{fixed} + c_{ik\ell}^{ship} + \gamma^{+} d_{k\ell}^{+} + \gamma^{-} d_{k\ell}^{-}) z_{ik\ell} - \sum_{k \in \mathcal{K}} \sum_{\ell \in \mathcal{L}} \beta_k w_{k\ell} \right) \quad (24)$$

$$\begin{aligned} \text{s.t.} \quad & \sum_{i \in \mathcal{I}} z_{ik\ell} \geq 2 - N(1 - y_{k\ell}) \\ & \sum_{i \in \mathcal{I}} z_{ik\ell} \leq 1 + N y_{k\ell} \\ & w_{k\ell} \leq M_{k\ell} y_{k\ell} \\ & w_{k\ell} \leq \sum_{i \in \mathcal{I}} c_{ik\ell}^{ship} z_{ik\ell} + (1 - y_{k\ell}) M_{k\ell}, \quad \forall k \in \mathcal{K}, \ell \in \mathcal{L}, \\ & w_{k\ell} \geq \sum_{i \in \mathcal{I}} c_{ik\ell}^{ship} z_{ik\ell} - (1 - y_{k\ell}) M_{k\ell} \\ & y_{k\ell} \in \{0, 1\} \\ & w_{k\ell} \geq 0 \end{aligned} \quad (25)$$

where N and $M_{k\ell}$ are large constants for the big-M constraints, with their strictest values being $\sum_{i \in \mathcal{I}} q_i + 2$ and $\sum_{i \in \mathcal{I}} c_{ik\ell}^{ship} q_i$, respectively.

F. Applying the C-RO-B to CSOFP

To successfully apply the budgeted interval uncertainty set, the uncertainty vector in the objective function $g(\mathbf{z}, \tilde{\mathbf{d}})$ should be element-wise positive. However, in the case of CSOFP, this requirement was not met due to the asymmetric penalty costs associated with deviations. Instead, the uncertainty in the problem can be represented by the vector of total costs. Let this uncertain cost vector be $\tilde{\mathbf{c}} = (\tilde{c}_{ik\ell})_{i \in \mathcal{I}, k \in \mathcal{K}, \ell \in \mathcal{L}}$, where each $\tilde{c}_{ik\ell} = (c_{\ell}^{fixed} + c_{ik\ell}^{ship} + \gamma^{+} \tilde{d}_{k\ell}^{+} + \gamma^{-} \tilde{d}_{k\ell}^{-}) \geq 0$ is the sum of fulfillment costs and deviation penalties for the order.

Substituting $\tilde{\mathbf{c}}$ leads to:

$$\min_{\mathbf{z} \in \mathcal{Z}} \max_{\tilde{\mathbf{c}} \in \mathcal{U}_b(\mathbf{s})} \left(\sum_{i \in \mathcal{I}} \sum_{k \in \mathcal{K}} \sum_{\ell \in \mathcal{L}} \tilde{c}_{ik\ell} z_{ik\ell} - \sum_{k \in \mathcal{K}} \sum_{\ell \in \mathcal{L}} \beta_k w_{k\ell} \right). \quad (26)$$

Given that the prediction interval for each $\tilde{d}_{k\ell}$ is $[\underline{d}_{k\ell}, \underline{d}_{k\ell o} + \hat{d}_{k\ell}]$, where $\underline{d}_{k\ell}$ and $(\underline{d}_{k\ell} + \hat{d}_{k\ell})$ are the estimated lower and upper quantiles of the deviation for the carrier-location pair (k, ℓ) , the prediction interval for \tilde{c} can be expressed as:

$$[\underline{\xi}_{ik\ell}, \underline{\xi}_{ik\ell} + \hat{\xi}_{ik\ell}] = c_\ell^{fixed} + c_{ik\ell}^{ship} + \begin{cases} [\gamma^- \underline{d}_{k\ell}, \gamma^- (\underline{d}_{k\ell} + \hat{d}_{k\ell})^-] & \text{if } \underline{d}_{k\ell} + \hat{d}_{k\ell} \leq 0 \\ [0, \max\{\gamma^- \underline{d}_{k\ell}, \gamma^+ (\underline{d}_{k\ell} + \hat{d}_{k\ell})\}] & \text{if } \underline{d}_{k\ell} \leq 0, \underline{d}_{k\ell} + \hat{d}_{k\ell} \geq 0 \\ [\gamma^+ \underline{d}_{k\ell}, \gamma^+ (\underline{d}_{k\ell} + \hat{d}_{k\ell})] & \text{if } \underline{d}_{k\ell} \geq 0 \end{cases} \quad (27)$$

Let $B \in [0, (|\mathcal{K}||\mathcal{L}|)]$ be the uncertainty budget. The contextual budgeted interval uncertainty set $\mathcal{U}_b(\mathbf{s})$ is expressed as follows:

$$\mathcal{U}_b(\mathbf{s}, B) = \{\boldsymbol{\xi} \in \mathbb{R}^{(|\mathcal{I}||\mathcal{K}||\mathcal{L}|)} : \xi_{ik\ell} = \underline{\xi}_{ik\ell} + \hat{\xi}_{ik\ell} \delta_{k\ell}, \sum_{k \in \mathcal{K}, \ell \in \mathcal{L}} \delta_{k\ell} \leq B, \boldsymbol{\delta} \in [0, 1]^{(|\mathcal{K}||\mathcal{L}|)}\}. \quad (28)$$

Then, with fixed \mathbf{z} , the inner maximization problem of Problem (26) becomes:

$$\max \sum_{i \in \mathcal{I}} \sum_{k \in \mathcal{K}} \sum_{\ell \in \mathcal{L}} \hat{\xi}_{ik\ell} z_{ik\ell} \delta_{k\ell} \quad (29)$$

$$\text{s.t.} \quad \sum_{k \in \mathcal{K}} \sum_{\ell \in \mathcal{L}} \delta_{k\ell} \leq B \quad (30)$$

$$\delta_{k\ell} \in [0, 1], \quad \forall k \in \mathcal{K}, \ell \in \mathcal{L}. \quad (31)$$

The robust counterpart of Problem (26) is formulated as follows:

$$\begin{aligned} \min_{\mathbf{z} \in \mathcal{Z}} \quad & \left(\sum_{i \in \mathcal{I}} \sum_{k \in \mathcal{K}} \sum_{\ell \in \mathcal{L}} \xi_{ik\ell} z_{ik\ell} - \sum_{k \in \mathcal{K}} \sum_{\ell \in \mathcal{L}} \beta_k w_{k\ell} + \pi B + \sum_{k \in \mathcal{K}} \sum_{\ell \in \mathcal{L}} \lambda_{k\ell} \right) \\ \text{s.t.} \quad & \pi + \lambda_{k\ell} \geq \hat{\xi}_{ik\ell} z_{ik\ell}, \quad \forall i \in \mathcal{I}, k \in \mathcal{K}, \ell \in \mathcal{L} \\ & \pi \geq 0 \\ & \lambda_{k\ell} \geq 0, \quad \forall k \in \mathcal{K}, \ell \in \mathcal{L}, \end{aligned} \quad (32)$$

where π and $(\lambda_{k\ell})_{k \in \mathcal{K}, \ell \in \mathcal{L}}$ are the dual variables of Constraints (30) and (31), respectively.

G. Probabilistic Multi-Class Classification Using Ensemble Learning

RF leverages multiple classification trees trained on different random subsets of the data, making predictions by averaging the results (Breiman 2001). Let $\mathcal{R}_1^{(t)}, \dots, \mathcal{R}_R^{(t)}$ correspond to the partitioned regions of the t -th tree. Given covariates \mathbf{s} , the predicted probability for class c in an RF classifier is:

$$\hat{p}_c(\mathbf{s}) = \frac{1}{T} \sum_{t=1}^T \frac{\sum_{r=1}^R \mathbf{1}\{\mathbf{s} \in \mathcal{R}_r^{(t)}\} \cdot \mathbf{1}\{d = \xi_c\}}{\sum_{r=1}^R \mathbf{1}\{\mathbf{s} \in \mathcal{R}_r^{(t)}\}}. \quad (33)$$

In contrast, GBT build classification trees sequentially, where each new tree is trained to optimize a loss function based on the residual errors of the previous trees (Friedman 2001). Let R be the number of boosting iterations. Given covariates \mathbf{s} , for the r -th tree where $r \in [R]$, let $h_r(\mathbf{s})$ be the prediction and γ_{cr} be the weight for class c . The predicted probability for class c in a GBT classifier is obtained using the softmax function of the log-odds:

$$\hat{p}_c(\mathbf{s}) = \frac{e^{G_c(\mathbf{s})}}{\sum_{c'=1}^C e^{G_{c'}(\mathbf{s})}}, \quad (34)$$

with the log-odds defined as:

$$G_c(\mathbf{s}) = \sum_{r=1}^R \gamma_{cr} h_r(\mathbf{s}). \quad (35)$$

H. Point Prediction ML Models

The regression models employed to generate point predictions are presented below.

1. Linear Regression (LinReg): LinReg solves the Ordinary Least Squares (OLS) problem.
2. Ridge Regression (Ridge): Ridge adds an L_2 norm regularization term to the coefficients obtained from OLS.
3. Least Absolute Shrinkage and Selection Operator Regression (Lasso): Lasso adds an L_1 norm regularization term to the coefficients obtained from OLS.
4. Random Forest (RF-Reg): RF-Reg operates similarly to the Random Forest classifier described in Section G, but it builds a collection of regression trees instead.
5. Gradient Boosted Trees (CatBoost-Reg and XGBoost-Reg): Two versions of Gradient Boosted Trees (GBT) are implemented for regression. These GBT models are similar to the GBT classifiers described in Appendix G, except they use regression trees. CatBoost-Reg is implemented using the CatBoost package, which builds symmetric trees and has native support for categorical features (Prokhorenkova et al. 2018). XGBoost-Reg is implemented using the XGBoost package (Chen and Guestrin 2016).

Table 5 Average Out-of-Sample MSE of Regression Models.

Model	LinReg	Ridge	Lasso	RF-Reg	CatBoost-Reg	XGBoost-Reg
MSE	2.324	2.324	3.149	1.791	1.668	1.666

I. Hyperparameters of the ML Models

Tables 6, 7, and 8 detail the hyperparameters and corresponding search spaces employed during the model selection and tuning processes for the ML algorithms considered in this study.

J. Evaluation of the Simulator

The simulator is compared against a baseline that uses multinomial logistic regression (MLR), a common approach in the literature (Salari et al. 2022).

Table 9 reports the average CRPS across all carriers. The proposed calibrated MC-CLF simulator achieves a CRPS of 0.314, compared with 0.779 for the MLR baseline, indicating a substantial improvement in distributional accuracy at the individual-instance level.

Figure 15 overlays each simulator’s joint predicted distribution on the true empirical distribution from the test set. The proposed calibrated MC-CLF simulator closely matches the empirical mass at zero deviation and reproduces both early- and late-delivery tails, whereas the MLR baseline systematically overpredicts late deviations and underpredicts on-time deliveries.

Figure 16 presents three carrier-specific examples. In each case, the proposed calibrated MC-CLF simulator aligns tightly with the carrier’s empirical distribution across all deviation classes. By contrast, the MLR baseline exhibits clear misalignments—particularly in the majority classes and tails—underscoring the proposed simulator’s superior ability to capture carrier-level heterogeneity.

K. Additional Details on Computational Scalability

Tables 10 and 11 provide a comprehensive comparison of objective values and computation times across different instance categories for the six proposed CSO methods.

Table 6 Hyperparameters for Point Prediction Regression Models

Model	Hyperparameter	Range
Ridge	α (L_2 regularization)	$1e-4 \leq \alpha \leq 10.0$
Lasso	α (L_1 regularization)	$1e-4 \leq \alpha \leq 10.0$
RF-Reg	n_estimators	$100 \leq \text{n_estimators} \leq 1000$ (step: 100)
	max_depth	$3 \leq \text{max_depth} \leq 10$
	min_samples_split	$2 \leq \text{min_samples_split} \leq 10$
	min_samples_leaf	$1 \leq \text{min_samples_leaf} \leq 20$
CatBoost-Reg	iterations	$50 \leq \text{iterations} \leq 300$
	depth	$4 \leq \text{depth} \leq 10$
	learning_rate	$0.01 \leq \text{learning_rate} \leq 0.3$
	l2_leaf_reg	$1 \leq \text{l2_leaf_reg} \leq 10$
	bagging_temperature	$0.0 \leq \text{bagging_temperature} \leq 1.0$
	random_strength	$0.0 \leq \text{random_strength} \leq 10.0$
	border_count	$1 \leq \text{border_count} \leq 255$
	colsample_bylevel	$0.5 \leq \text{colsample_bylevel} \leq 1.0$
XGBoost-Reg	n_estimators	$100 \leq \text{n_estimators} \leq 1000$ (step: 100)
	max_depth	$3 \leq \text{max_depth} \leq 10$
	learning_rate	$0.01 \leq \text{learning_rate} \leq 0.3$
	subsample	$0.5 \leq \text{subsample} \leq 1.0$
	colsample_bytree	$0.5 \leq \text{colsample_bytree} \leq 1.0$
	gamma	$0 \leq \text{gamma} \leq 5$
	reg_alpha	$0.0 \leq \text{reg_alpha} \leq 100.0$
	reg_lambda	$0.0 \leq \text{reg_lambda} \leq 100.0$
	min_child_weight	$1 \leq \text{min_child_weight} \leq 10$
	max_delta_step	$0 \leq \text{max_delta_step} \leq 10$
	colsample_bylevel	$0.5 \leq \text{colsample_bylevel} \leq 1.0$
	colsample_bynode	$0.5 \leq \text{colsample_bynode} \leq 1.0$

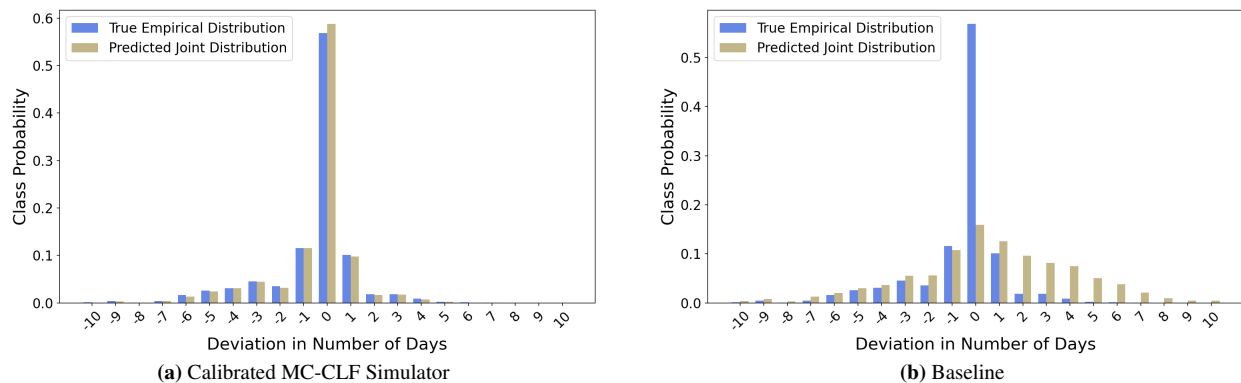


Figure 15 Overall Joint Predicted Distribution of the Simulators vs. the True Empirical Distribution

K.1. Sample Size Selection: Balancing Solution Quality and Computational Efficiency

Figures 17 and 18 illustrate the trade-off between average realized objective value and computation time for the two C-SAA methods.

Table 7 Hyperparameters for Classification Models

Model	Hyperparameter	Range
MLR	C (regularization)	$1e-4 \leq C \leq 1e2$
Classification Tree	max_depth	$3 \leq \text{max_depth} \leq 10$
	min_samples_leaf	$10 \leq \text{min_samples_leaf} \leq 30$ (step: 5)
RF-MC-CLF	n_estimators	$600 \leq \text{n_estimators} \leq 1000$ (step: 200)
	max_depth	$3 \leq \text{max_depth} \leq 10$
	min_samples_split	$2 \leq \text{min_samples_split} \leq 10$
	min_samples_leaf	$10 \leq \text{min_samples_leaf} \leq 30$ (step: 5)
CatBoost-MC-CLF	iterations	$50 \leq \text{iterations} \leq 300$
	depth	$4 \leq \text{depth} \leq 10$
	learning_rate	$0.01 \leq \text{learning_rate} \leq 0.3$
	l2_leaf_reg	$1 \leq \text{l2_leaf_reg} \leq 10$
	bagging_temperature	$0.0 \leq \text{bagging_temperature} \leq 1.0$
	random_strength	$0.0 \leq \text{random_strength} \leq 10.0$
	border_count	$1 \leq \text{border_count} \leq 255$
colsample_bylevel	$0.5 \leq \text{colsample_bylevel} \leq 1.0$	

Table 8 Hyperparameters for Quantile Regression Models

Model	Hyperparameter	Range
Regression Tree	max_depth	$3 \leq \text{max_depth} \leq 10$
	min_samples_leaf	$10 \leq \text{min_samples_leaf} \leq 30$ (step: 10)
QRF	n_estimators	$600 \leq \text{n_estimators} \leq 1000$ (step: 200)
	max_depth	$3 \leq \text{max_depth} \leq 10$
	min_samples_split	$2 \leq \text{min_samples_split} \leq 10$
	min_samples_leaf	$10 \leq \text{min_samples_leaf} \leq 30$ (step: 5)

Table 9 Average In-Sample CRPS Across All Carriers.

Model	Calibrated MC-CLF Simulator	MLR Simulator (Baseline)
CRPS	0.314	0.779

Table 10 Realized Average (\pm 95% CI margin of error) and Worst-Case Objective Values Across Instance Categories.

Instance	C-SAA-CLF		C-SAA-QRF		C-RO-B-CLF		C-RO-B-QRF		C-RO-D-CLF		C-RO-D-QRF	
	Avg.	Worst	Avg.	Worst	Avg.	Worst	Avg.	Worst	Avg.	Worst	Avg.	Worst
Small	0.821 ± 0.003	0.790	0.848 ± 0.004	0.813	0.851 ± 0.004	0.794	0.871 ± 0.003	0.813	0.936 ± 0.004	0.757	0.920 ± 0.004	0.766
Medium	0.799 ± 0.008	0.932	0.806 ± 0.009	0.925	0.797 ± 0.009	0.834	0.815 ± 0.009	0.821	0.890 ± 0.010	0.822	0.883 ± 0.009	0.825
Large	0.847 ± 0.012	1.032	0.871 ± 0.017	1.055	0.823 ± 0.014	0.982	0.836 ± 0.016	0.981	0.910 ± 0.017	0.972	0.904 ± 0.014	0.973
Total	0.820 ± 0.003	0.823	0.844 ± 0.003	0.842	0.842 ± 0.003	0.811	0.861 ± 0.003	0.824	0.928 ± 0.003	0.779	0.914 ± 0.003	0.787

Table 11 Computation Time Statistics (in seconds) Across Instance Categories.

Instance	C-SAA-CLF			C-SAA-QRF			C-RO-B-CLF			C-RO-B-QRF			C-RO-D-CLF			C-RO-D-QRF		
	Mean	Std	Max	Mean	Std	Max	Mean	Std	Max	Mean	Std	Max	Mean	Std	Max	Mean	Std	Max
Small	1.620	2.267	28.021	1.619	2.271	28.185	0.016	0.024	0.374	0.015	0.024	0.740	0.199	0.301	5.475	0.192	0.275	3.161
Medium	27.831	10.245	107.347	27.896	10.305	107.949	0.281	0.106	0.860	0.275	0.107	0.857	3.229	2.008	39.222	3.145	1.694	22.426
Large	59.266	22.590	182.401	59.720	22.875	188.076	0.698	0.322	2.856	0.732	0.395	2.811	7.683	7.056	111.188	7.070	3.609	29.129
Total	8.974	17.433	182.401	9.010	17.555	188.076	0.096	0.203	2.856	0.097	0.217	2.811	1.101	2.791	111.188	1.045	2.186	29.129

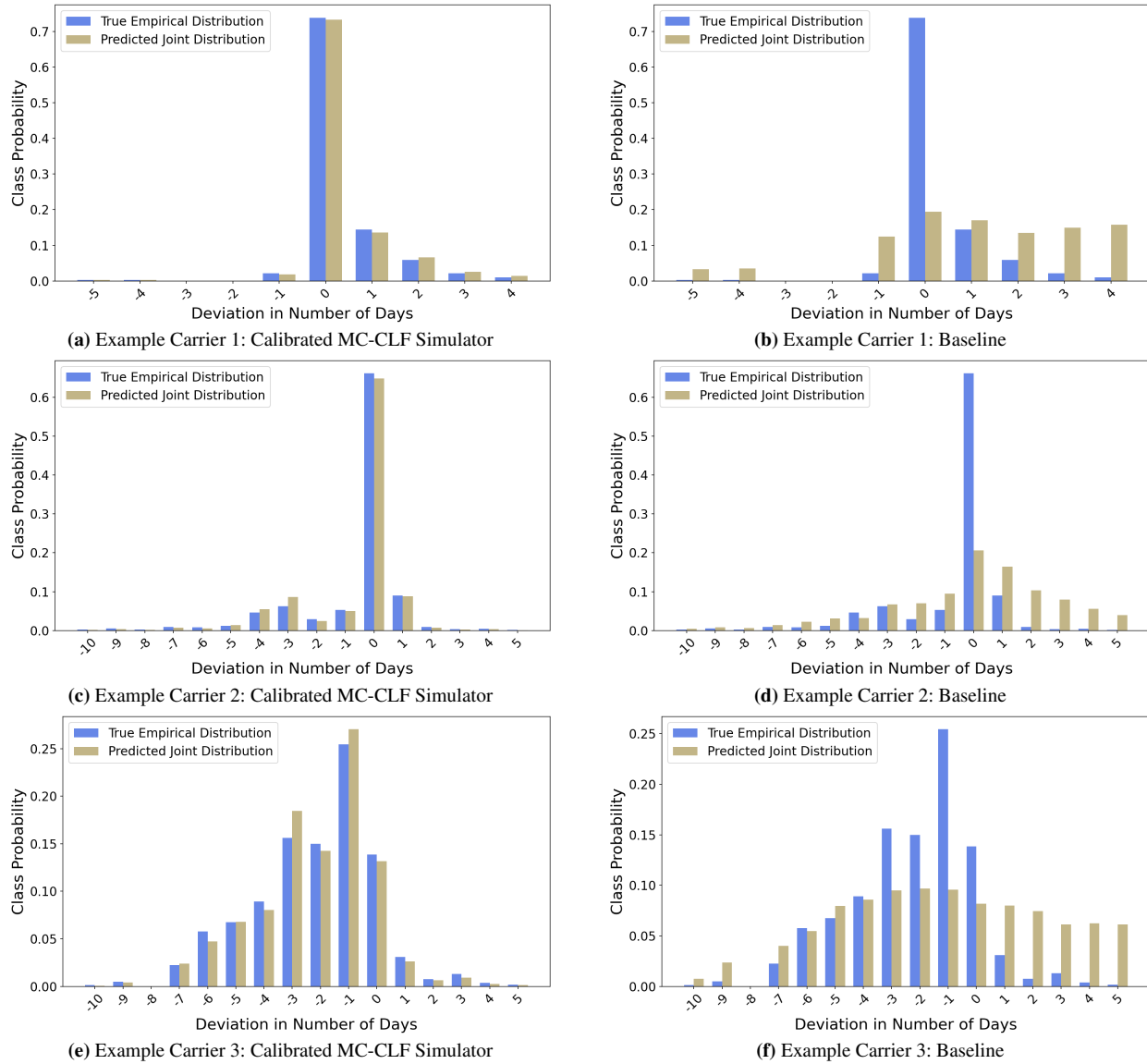


Figure 16 Selected Carrier Examples: Joint Predicted Distribution of the Simulators vs. the True Empirical Distribution

Similarly, Figures 19 and 20 depict the trade-off between worst-case realized objective value and computation time for the two C-RO-D methods.

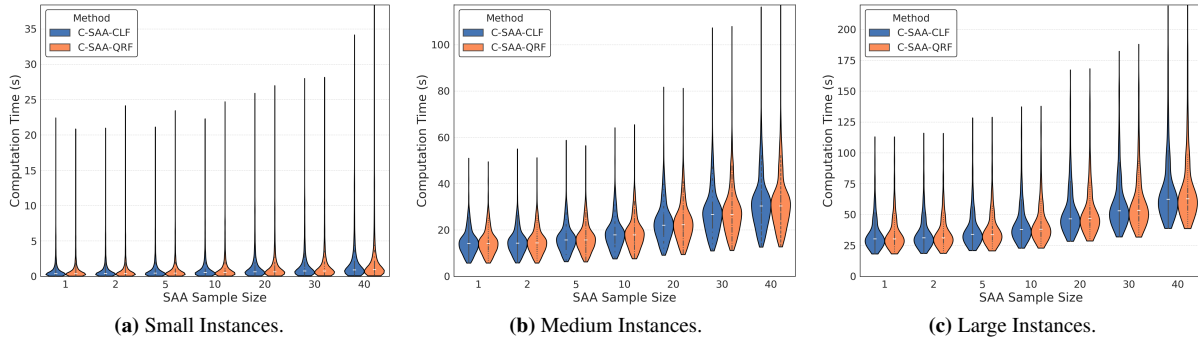


Figure 17 Computation Time by C-SAA Sample Size.

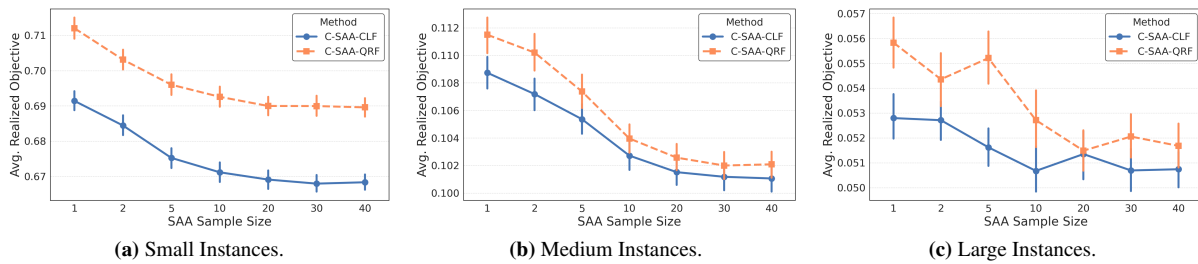


Figure 18 Average Realized Objective Value by C-SAA Sample Size.

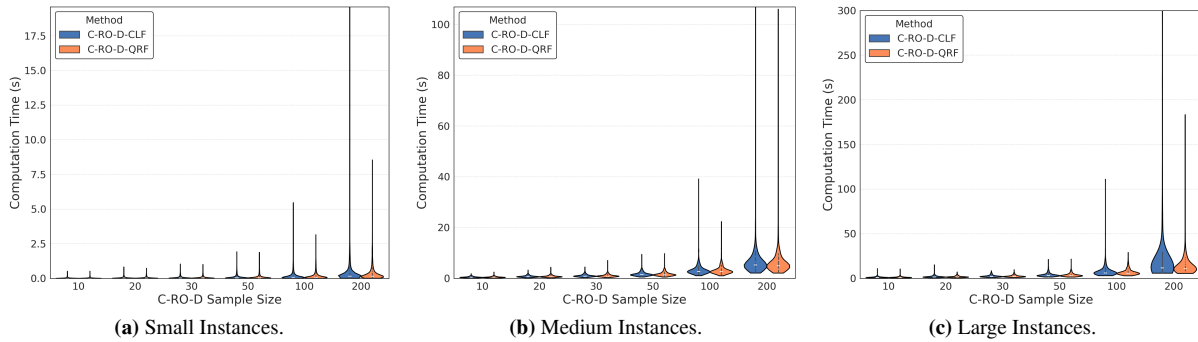


Figure 19 Computation Time by C-RO-D Sample Size.

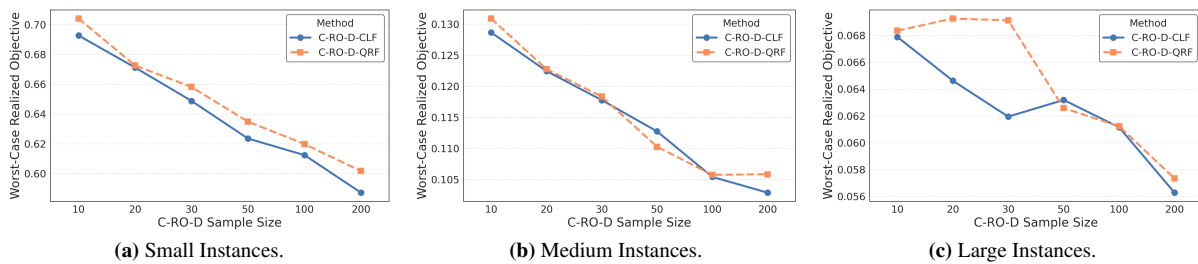


Figure 20 Worst-Case Realized Objective Value by C-RO-D Sample Size.